Automated cross-sectional analysis of trained, severely atrophied and recovering rat skeletal muscles using MyoVision 2.0

Mark R Viggars[1,2,3*], Yuan Wen[4,5,6*], Charlotte A Peterson[4,5,] Jonathan C Jarvis[1]

[1]*Research Institute for Sport and Exercise Sciences, Liverpool John Moores University, Liverpool, UK.*

[2]*Department of Physiology and Functional Genomics, University of Florida, Gainesville, Florida.*

[3]*Myology Institute, University of Florida, Gainesville, Florida.*

[4]*Department of Physiology, College of Medicine, University of Kentucky, Lexington, Kentucky.*

[5]*Center for Muscle Biology, University of Kentucky, Lexington, Kentucky.*

[6]*MyoAnalytics, LLC, Lexington, Kentucky.*

**Joint First Authors*

Correspondence: Mark Viggars (m.viggars@ufl.edu) Physical Address: [2]Department of Physiology and Functional Genomics, University of Florida, Gainesville, Florida, USA, 32608.

Abstract:

The number of myonuclei within a muscle fiber is an important factor in muscle growth, but its regulation during muscle adaptation is not well understood. We aimed to elucidate the timecourse of myonuclear dynamics during endurance training, loaded and concentric resistance training, and nerve silencing-induced disuse atrophy with subsequent recovery. We modified tibialis anterior muscle activity in free-living rats with electrical stimulation from implantable pulse generators, or with implantable osmotic pumps delivering tetrodotoxin (TTX) to silence the motor nerve without transection. We used the updated, automated software MyoVision to measure fiber type-specific responses in whole tibialis anterior cross-sections (~8000 fibers each). Seven days of continuous low frequency stimulation (CLFS) reduced muscle mass (-12%), increased slower myosin isoforms and reduced IIX/IIB fibers (-32%) and substantially increased myonuclei especially in IIX/IIB fibers (55.5%). High load resistance training (Spillover), produced greater hypertrophy (~16%) in muscle mass and fiber cross-sectional area (CSA) than low load resistance training (concentric, ~6%) and was associated with myonuclear addition in all fiber types (35-46%). TTX-induced nerve silencing resulted in progressive loss in muscle mass, fiber CSA, and myonuclei per fiber cross-section (-50.7%, -53.7%, -40.7%, respectively at 14 days). Myonuclear loss occurred in a fiber type-independent manner, but subsequent recovery during voluntary habitual activity suggested that type IIX/IIB fibers contained more new myonuclei during recovery from severe atrophy. This study demonstrates the power and

accuracy provided by the updated MyoVision software and introduces new models for studying myonuclear dynamics in training, detraining, retraining, repeated disuse, and recovery.

New & Noteworthy

We introduce new models for studying fiber-type specific myonuclear dynamics in muscle training, detraining, retraining, disuse, and recovery. We show that the various fiber types do not respond identically, and that myonuclear number changes during adaptation. We also critically assess an updated version of MyoVision automated image analysis software, to quantify whole muscle immunofluorescent microscopical images in a faster and less computer intensive manner. MyoVision remains open source and freely available with more user-controlled features.

Introduction:

Skeletal muscle is highly responsive to changes in mechanical forces. Additional load is a key regulator of muscle hypertrophy, and muscle unloading is a trigger for muscle atrophy (1). There are several potential adaptive mechanisms that may allow trained muscle to recover faster than untrained muscle from periods of catabolism including epigenetic modifications (2, 3) and/or miRNA levels and myonuclear shape (4). Myonuclear number itself has also been suggested as a potentially stable indicator of previous episodes of hypertrophy (5). Myonuclei can alter their transcriptional activity in response to mechanical cues, such as those caused by exercise, as well as to internal factors such as proximity to other myonuclei (6-9). Increase in synthetic activity following exercise probably reflects a shift in mRNA expression to reprogram cellular phenotype in response to the demands imposed on the muscle fiber, as well as increasing rRNA expression to increase translational efficiency and capacity (6, 10, 11).

To support transcriptional demands during muscle remodelling, it may be necessary to increase the number of myonuclei per unit cell volume. Since muscle fibers are post-mitotic, this is achieved through muscle stem cells (satellite cells), which can proliferate and then fuse to myofibers adding

new myonuclei. The presence of satellite cells is not completely obligatory for short term load-induced hypertrophy (12), or androgen-induced hypertrophy (13), but in adult skeletal muscle (14), their depletion alters the myonuclear transcriptome and blunts adaptation to exercise, proprioception and exercise capacity (15-17). Satellite cells also play an important role in muscle homeostasis by communicating with endothelial and fibroadipogenic progenitor cells in skeletal muscle, as well as with the myonuclei themselves (18-21). However, whether all nuclei or newly added myonuclei are permanent and able to act as a cellular memory (5), or whether they can be lost through caspase dependent and caspase-independent (Endonuclease G) mechanisms is yet to be fully confirmed (22).

Training followed by subsequent 'detraining' has revealed that different individual muscles show a variety of responses. Six months of detraining after 2 months of progressive weighted wheel running (PoWeR) showed that the fiber type shifts, fiber hypertrophy and increases in myonuclear number caused by training were reversed after detraining in the gastrocnemius and plantaris muscles (4, 23). By contrast, the soleus muscle did not lose PoWeR adaptations following detraining and type I fibers showed higher myonuclear content with no increase in fiber size. Clearly, the loss or addition of myonuclei following training and detraining is a complicated phenomenon with the data indicating that there are large differences between responses according to training model, species, age, muscle group and muscle fiber type (24). How muscle disuse compares with detraining and whether recovery from disuse atrophy is comparable to training-induced hypertrophy in terms of myonuclear dynamics are currently unknown. The requirement for new myonuclei and whether those nuclei are retained may be controlled by a combination of motor activity, oxidative capacity, and tonic stretch.

Currently, the most direct and accurate methods to assess myonuclei number are myonuclear counts in single extracted myofibers, or intravital imaging of the small number of myonuclei visible in superficial fibers (7, 25-28). However, these methods are labor intensive and may not represent the population of myonuclei within a muscle with typically thousands to tens of thousands of fibers

with complex architectural properties, different resting/working lengths, and differing activation patterns. Thus, assessing entire whole muscle cross-sections via immunohistochemical labelling as we have done here remains the most accessible and unbiased approach if performed by automatic, high throughput image analysis.

In this investigation, we combined the improved capabilities of MyoVision automated histological analysis software to characterize adaptive changes in myonuclei number per fiber on whole cross-sections of tibialis anterior, each containing between 6000 and 10,000 fibers, in 3 adaptive conditions: 1) A time course of programmed daily resistance exercise: high load contractions, achieved by a technique we call 'Spillover stimulation' because the supramaximal stimulation of the common peroneal nerve is adjusted to 'spill over' to activate some of the antagonistic motor units of the plantarflexors supplied by the tibial nerve) vs. unloaded contractions (concentric) to induce hypertrophy, 2) continuous low frequency stimulation (CLFS) to induce an endurance-trained phenotype and 3) disuse atrophy by means of reversible nerve silencing with subsequent recovery (29, 30). Our objective for each paradigm of muscle adaptation was to understand changes in cross sectional area for each fiber type and whether this correlated with myonuclear content. We hypothesized that following our exercise training protocols, as all muscle fibers are activated synchronously, the extent of growth and myonuclear accretion may reflect the total activity time/loading similarly in all fiber types. Furthermore, as our atrophy model prevents propagation of action potentials in all muscle fibers, myonuclei might be lost in a fiber type-independent manner, but the recovery by habitual voluntary activity might produce myonuclear accretion according to the normal graded recruitment of muscle fibers.

Methods:

Experimental Design

The animal experiments were conducted under the provisions of the Animals (Scientific Procedures) Act 1986 and approved by the British Home Office (PPL 40/3280). Male Wistar rats were group-

housed with 2-3 per cage maintaining an alternating 12 h light 12 h dark cycle. The mean age of all rats was 18 ± 2 weeks upon euthanasia. All animals survived their elected experimental timecourse. Pre-surgical and post experimental weights for each group can be found in Table 2.

INSERT TABLE 2 HERE

INSERT FIGURE 1 HERE

Resistance Training Protocols & Pattern

Animals received 1 session per day of high load (Spillover) or low load (concentric) resistance training (RT) in the left hind-limb via stimulation from an implanted pulse generator (IPG) as previously described (30), for 2 (*n*=4), 10 (*n*=6), 20 (*n*=6), or 30 days (*n*=8), or underwent sham surgery (*n*=6). Briefly, for high load (Spillover) exercise to elicit slight stretch under load, the dorsiflexor muscles, tibialis anterior (TA) and extensor digitorum longus (EDL), received supramaximal activation via a cathode placed underneath the common peroneal nerve (CPN), while the anode was positioned underneath the tibial nerve. Stimulation current was adjusted by remote programming, to recruit enough of the gastrocnemius, plantaris and soleus (plantarflexor muscles) to provide appropriate resistance against the contraction of the dorsiflexors. In an additional group (*n*=6), animals received 1 session per day of unresisted (concentric) contractions of the dorsiflexors for 30 days by placing both electrodes under the CPN during implantation so there was no activation of the plantarflexor muscles, and the dorsiflexors contracted against a low load.

Daily training was delivered during the first hour of the inactive light phase automatically by the IPG and consisted of an initial 10 seconds of preparatory stimulation at a low frequency (F = 4Hz, phase width =258 µs, current = approximately 1 mA), followed by 5 sets of 10 tetanic contractions at 100 Hz. Each contraction lasted for 2s with 2s rest between contractions and 2.5 minutes of rest between sets. The stimulation was delivered only in the left hind-limb, so muscles of the right hind-

129 limb acted as unstimulated contralateral controls. Stimulation with these settings and the amplitude
130 chosen to balance dorsiflexion and plantarflexion described above was well-tolerated by all animals
131 without further anaesthesia or sedation. Regular observations during daily training across the time
132 course revealed no adverse behavioural signs.

133 *Continuous Low Frequency Stimulation (CLFS)*

134 As previously described (29, 31), the ankle dorsiflexors of the left hind-limb were continuously
135 stimulated (24 h per day), at 20Hz for 7 days (*n*=6). This pattern has previously been shown to induce
136 a transformation from the control fast phenotype towards a slower more oxidative phenotype in the
137 dorsiflexor muscles characteristic of endurance training (32).

138 *Electrical Stimulation Surgical Procedure*

139 Animals were anaesthetised during implant procedures by inhalation of a gaseous mixture of
140 isoflurane in oxygen at approximately 3% for induction and 1-2% for maintenance. Once
141 anaesthetised, a subcutaneous injection of Enrofloxacin (5mg/kg^{-1} body mass (Baytril®) and an
142 intramuscular injection of Buprenorphine (0.05mg/kg^{-1} body mass) (Temgesic, Indivior, Slough, UK)
143 into the right quadriceps was administered with strict asepsis maintained throughout the procedure.
144 Nerve stimulation was delivered from silicone-encapsulated implanted pulse generators (IPGs)
145 (MiniVStim 12B, Competence Team for Implanted Devices, Center for Medical Physics and
146 Biomedical Engineering, Medical University Vienna, Austria) which could be programmed remotely
147 by a radio frequency link. The devices were implanted into the abdominal cavity accessed by a
148 lateral incision through the skin and peritoneum, between the rib cage and pelvis on the left side of
149 the animal. A polyester mesh attached to the IPG was incorporated into the suture line closing the
150 peritoneum, securing the device against the abdominal wall. Two PVC-insulated stainless-steel
151 electrode leads (Cooner Sales Company, Chatsworth, California, U.S.A.) with terminal conductive
152 loops, were fed through the peritoneal incision and tunnelled under the skin to the lateral side of the
153 upper left hind-limb. A second incision was made through the skin and biceps femoris muscle to give

154 access to the CPN under which the cathode was placed (to stimulate the dorsiflexors). The anode
155 was either placed alongside the cathode to stimulate the CPN alone and thus to produce unresisted
156 (concentric) contractions or placed in the muscular tissue deep to the tibial nerve about 5mm distal
157 to its bifurcation from the sciatic nerve to allow Spillover stimulation to produce additional partial
158 activation of the plantarflexors to resist the contraction of the dorsiflexors, resulting in a loaded
159 contraction. All incisions were closed in layers and 3-7 days were allowed for recovery from surgery
160 before the start of the training protocol. Once programmed, the stimulators ran autonomously to
161 provide the selected activation pattern over the course of the experiment.

162 *Nerve Silencing-Induced Disuse by Tetrodotoxin & Recovery Protocols*

163 INSERT FIGURE 2 HERE

164 The CPN, the motor nerve responsible for contraction of the TA and EDL, was silenced with
165 tetrodotoxin (TTX) for pre-set periods of 3 days (*n*=4), 7 days (*n*=6), or 14 days (*n*=6). Atrophy of the
166 dorsiflexors was produced without signs of fiber necrosis or denervation assessed by H&E staining. A
167 separate group was used to assess recovery after 14 days of tetrodotoxin (TTX) treatment. Osmotic
168 pumps were appropriately loaded so that the TTX infusion was exhausted after 14 days, and nerve
169 activity could resume during 7 days of muscle recovery via habitual physical activity (*n*=6). Pumps
170 were weighed before implantation and again after explant to confirm that the expected volume of
171 TTX had been delivered over the time course of the experiment. Muscle mass data from these
172 groups has previously been reported (29).

173 *Tetrodotoxin Administration Surgical Procedure*

174 Animals were anaesthetised as previously described for the implantable stimulator surgeries. A
175 miniosmotic pump (Mini Osmotic Pump 2002; Alzet, Cupertino, CA, USA) was implanted
176 subcutaneously in the scapular region. Silicone tubing was tunnelled under the skin to the site of the
177 CPN. A second incision was made laterally through the skin, just proximal to the knee joint and bicep

femoris muscle (posterior compartment of the thigh) in order to give access to the CPN responsible for action of the dorsiflexors. A silicone cuff extending from the silicone tubing was placed around the nerve. All incisions were closed in layers. The miniosmotic pump (Mini Osmotic Pump 2002; Alzet, Cupertino, CA, USA) delivered TTX, a sodium channel blocker that prevents generation and propagation of action potentials at the CPN of the left hind-limb. The osmotic pump successfully delivered 0.5µl/h TTX (350mg/ml in sterile 0.9% saline), continuously blocking ankle dorsiflexion, while maintaining normal voluntary plantarflexion via the tibial nerve. Disuse of the dorsiflexors by this means produces progressive atrophy (29). The welfare and mobility of the rats was checked daily by animal welfare staff. There was little disturbance to mobility, but sometimes 'foot drop' was observed, a gait abnormality characterised by dropping of the forefoot due to the inhibition of dorsiflexion.

Rat muscle sampling and preservation

Animals were humanely sacrificed using rising concentrations of carbon dioxide (at a displacement rate of 50% of the animals' home cage volume per minute), followed by cervical dislocation. TA muscles from both hind limbs were immediately harvested, cleaned of excess connective tissue, and weighed. The mid-belly of the TA was cut out, placed on cork for transverse sectioning and frozen in melting isopentane above liquid nitrogen for later immunohistochemical analysis.

Immunohistochemistry

Muscle samples were sectioned at 10µm using an OTF5000 Cryostat (Bright Instruments, UK) onto Thermo Scientific™ SuperFrost Plus™ Adhesion slides (Thermo Fisher Scientific Inc, Waltham, USA). Muscle cross-sections were labelled with primary antibodies against dystrophin (MANDYS8-8H11 or a polyclonal dystrophin antibody (1:200)) to demarcate the inside of the sarcolemma for all the experimental samples. Fiber type analysis was performed on TA muscles within the 30 days loaded RT, 30 days concentric RT, 7 days 20Hz CLFS, 14 days atrophy and 14 days atrophy with 7 days recovery groups, through labelling of dystrophin, as well as BA-D5 (anti myosin type I) and SC-71

(anti myosin type IIA) hybridoma supernatants (1:100), diluted in immunobuffer (IB) overnight and then washed 3 x 10 minutes in IB. Unstained muscle fibers were later measured as IIX/IIB fibers. Appropriate secondary antibodies with specific Ig fragments were diluted in IB for 2 hours (1:500), followed by 3 x 10 minutes in IB. IB consists of 50mM glycine (Merck 1.02401_1000), 0.25% BSA, 0.03% saponin (Sigma 100g S-7900), and 0.05% sodium azide in phosphate buffered saline (PBS, 10mM phosphate pH 7.4, 150mM NaCl).

For all cross-sections, following incubation with primary and secondary antibodies (Table 1), nuclei were labelled with DAPI (D1306, Thermofisher Scientific) at a concentration of 30nM diluted in PBS for 30 minutes, prior to 3 x 5-minute washes in PBS. Coverslips were then mounted onto cross-sections with VECTASHIELD® Antifade Mounting Medium (Vector Laboratories, UK). Hematoxylin and Eosin (H&E) staining was also performed on serial or 'near serial' sections within ~10-60µm, to check for evidence of damage, de/regeneration and fiber loss by independent researchers.

Table 1: Primary antibodies and appropriate corresponding secondary antibodies used.

INSERT TABLE 1 HERE

Imaging

Once labelled, whole muscle cross-sections were imaged using a widefield fluorescent microscope (Leica DMB 6000, Wetzlar, Germany) with a 10x objective. Multiple images were automatically stitched together using the tilescan feature in the Leica Application Suite.

MyoVision 2.0 Analysis:

MyoVision 2.0 introduced major upgrades to the original MyoVision software, but the fundamental workflow including fiber detection, fiber type classification, and myonuclear counting remained essentially the same as described previously (33). For fiber detection, the software uses the single

channel intensity image of dystrophin labelling as an input as well as the pixel scale (µm/pixel) to allow for calculation of mean fiber cross-sectional area in units of square micrometres. Following fiber detection, a single channel intensity image of immuno-labelled myosin heavy chain or nuclei can be provided to the software to classify fiber type or quantify myonuclei number. For each myofiber cytoplasmic region excluding the periphery, the mean myosin heavy chain immunofluorescence intensity was quantified on a scale of 0 to 1, with 1 being maximum signal for the section. Only fibers with mean myosin heavy chain intensity greater than 0.5 were classified as true for that particular fiber type. When analysing multiple fiber types, the image corresponding to each fiber type staining was analysed independently. Thus, a fiber classified as "negative" would represent false for all fiber types included in the analysis whereas a "hybrid" classification would indicate co-expression of at least two different myosin heavy chain isoforms within the same fiber. The criteria for myonuclear classification remain the same as in the previous version; specifically, a nuclear region with its centroid inside the fiber dystrophin border and at least 50% of its total area within the fiber cytoplasm is counted as a myonucleus.

A major upgrade to the software is the implementation of neural networks in fiber detection and fiber type classification steps. As summarized in Supplementary Figure 1, multiple steps in the previous MyoVision algorithm have been replaced with U-net models (34), which demonstrated superior performance in the segmentation of grayscale intensity based images of cells. The models were trained using annotated images of 256 by 256 pixels. Briefly, images of whole cross-sections were labelled as true for foreground (i.e. fiber boundary) and false for background (i.e. non-specific signals or staining artefacts). These images along with their ground truth label were separated into 256x256 pixel regions. The same image and ground truth label were then reduced by two-fold in size sequentially, and 256X256 pixel regions were extracted from the smaller images in a similar fashion as the original image. Reducing the image size allows for the model to learn at different image resolutions and different magnifications. Images representing 1x, 0.5x, and 0.25x along with their ground truth labels were used to train the weights of a U-net model for up to 100 epochs at 300

steps per epoch using Keras (v2.2.4) and Tensorflow (v1.13.1). Models were similarly trained for each step in the algorithm to replace the corresponding steps in the previous version of the software (Supplementary Figure 1). Of note, the previous software included the active contour algorithm by default, which expands the fiber contour as close to the inner edge of the dystrophin border as possible to allow for myonuclear counting. The previous version included a step that separated (shrank) certain cytoplasmic regions that were probably connected; thus, the active contour algorithm was applied to every fiber outline to expand the contour of the cytoplasmic space to the inner edge of the dystrophin border. This step had been relocated to the nuclear counting analysis exclusively due to its resource intensiveness and the fact that general fiber detection does not require such stringent delineation of the inner edge of the sarcolemma. This modification led to the same fiber cross-sectional area values, but a reduction in the defined 'cytoplasmic region' which is now slightly smaller (~5%) than the value estimated by the previous version of the software. This modification was favorable not only from a computational resource perspective, but also resulted in values more in line with various other approaches in the literature that do not include any myonuclear analysis. The software will be made freely available to the research community and additional documentation for the current version can be found on www.myoanalytics.com/myovision2. Together these modifications make it possible to analyses much larger images than was possible on the previous version of MyoVision and improve the access for the user to the calculated data for every fiber recognised in the image.

In addition, users now have control over circularity, solidity and eccentricity parameters for identifying fibers (Supplementary Figure 2), for analysis of different muscle phenotypes and extreme atrophic conditions. Other functionalities introduced in this upgrade include robust detection of whole cross-sections, batch processing of images for large projects, export of representative images from the software, exporting images from Olympus microscopes, adjusting images to control for background noise, and output of multiple shape descriptors for each fiber.

A total of 166 complete cross-sections of rat TA were generated by tile scanning and reconstructing to generate single image files for each muscle in our test and control groups. These were analyzed in the process of beta testing of the new software taking an average of 29.80 ± 4.87 minutes per cross-section for detection and analysis of fiber CSA, three fiber types and myonuclear number on a PC Specialist laptop, equipped with an Intel® Core™ i7-6700K CPU 4.00GHz processor and 64GB of RAM. Use of a CUDA-capable GPU having a Compute Capability of greater than 3.5 and 8GB or more dedicated memory would further increase the speed of image processing and analysis.

Manual Quantification versus Myovision 2.0 for assessing severely atrophied muscle fibers

Hematoxylin and Eosin (H&E) stained cross-sections were used for manual quantification of fiber number, which was performed on 5 self-selected fields of view containing (~450-600) muscle fibers with the most severe atrophy after 14 days of TTX treatment. Using the multi-point tool in Image-Pro Plus 5.1 software (Media Cybernetics, MD, USA), fiber number was counted and then compared with analysis by Myovision of the serial immunohistochemically labelled field of view, identified by means of landmarks such as blood vessels or distinctive connective tissues.

Statistics

Data are presented as the % change between the left experimental hind-limb and right internal contralateral control hind-limb for overall muscle mass (mg/kg bodyweight), fiber CSA, myonuclei per fiber cross-section and myonuclear domain across all experimental models, that is, the absolute difference (positive or negative) expressed as a percentage of the control value. The resultant percentage changes were then compared via one-way ANOVA, followed by Tukey's post-hoc analysis to confirm differences between groups. For fiber type-specific analysis, absolute values of fiber number, fiber type proportion, fiber CSA, myonuclei per fiber cross-section and myonuclear domain were compared between groups using one-way ANOVA's, followed by Tukey's post-hoc analysis to confirm differences between groups. Simple linear regression was also performed on % changes between muscle mass, fiber CSA, myonuclei per fiber cross-section and myonuclear domain size. For

the recovery group from TTX, co-efficient of variation was performed on values produced by expressing the 14 days TTX with 7-day recovery muscle values, as a percentage change from the mean 14-day TTX treatment values to show the extent of myonuclear addition as a % increase, rather than a % decrease from baseline. Significance was set at $P < 0.05$ for all statistical analyses, performed in GraphPad Prism 9.0 software. All data are presented as mean ± standard deviation (SD).

Results:

Tibialis anterior (TA) fiber type, number, size and myonuclear characteristics in control hind-limbs

We first sought to assess the fiber type composition, fiber cross-sectional area (CSA) and myonuclear-related characteristics of the rat TA muscle in 32 untreated control hind-limbs across all our experimental conditions. Although the TA is a predominately fast-twitch muscle, we pay particular attention to the more oxidative, slower myosin isoform-containing muscle fibers as they still make up approximately 25% of all muscle fibers at the mid-belly and therefore have functional significance. We note that myosin heavy chain profiles can change across the length of a muscle, and we only study the mid-belly, other longitudinal regions should be considered dependent on the muscle. Our data (Figure 3A) confirms previous measurements of fiber type percentages in rat TA with IIX/IIB fibers (75.7 ± 8.4%) representing a significantly higher population than all other measured fiber types (P <0.00001). While IIA fibers represented a significantly lower proportion of the TA muscle (21.29 ± 7.1%), they represented a significantly higher proportion than type I/IIA hybrids (3.09 ± 2.4%, P = <0.0001) or pure type I fibers (2.04 ± 1.1%, P = <0.0001), respectively. There was no significant difference between the proportion of type I and type I/IIA hybrid fibers, P= 0.859. As well as being the predominant fiber types in the TA, type IIX/IIB fibers also possess significantly higher mean fiber CSA (2380 ± 327μm^2) than all other fiber types measured (Figure 3B), P <0.00001. Type IIA mean fiber CSA (1399 ± 212μm^2), was significantly larger than both type I/IIA hybrid fiber CSA (1158 ± 208 μm^2, P = 0.0010) and type I fiber CSA (1180 ± 229 μm^2, P =0.0053). Furthermore,

there was no significant difference between type I/IIA hybrids and type I fiber CSA. Interestingly, there was no significant difference between any of the fiber types for the number of myonuclei per fiber cross-section (Figure 3C), with type I, I/IIA hybrids, IIA, and IIX/IIB fibers containing 0.96 ± 0.2, 1.01 ± 0.22, 1.09 ± 0.22, 1.03 ± 0.23 myonuclei per cross-section, respectively. As a result, myonuclear domain size, that is average cross-sectional area per nucleus, was significantly larger in type IIX/IIB fibers (2564 ± 1742μm^2) than all other fiber types measured, P <0.0001 (Figure 3D). There was no significant difference between type I (1417 ± 620μm^2), type I/IIA hybrids (1483 ± 727μm^2) and type IIA (1362 ± 544μm^2) myonuclear domain sizes. The mean total fiber number detected across all control TAs (n=32) was 8060 ± 1078 per TA (Figure 3E). Despite a large sample size, co-efficient of variation (CV) was still 13.38% for total fiber number, demonstrating the need for an internal contralateral control measurement. The CV of the difference in fiber number between left and right hind-limbs is only 5.04% from 63 pairs of TAs in this study. Total fiber number was not significantly different between any group or between the left experimental TA and right internal contralateral control TA after any treatment (P >0.05) (Figure 3E). Some variation was present between left and right hind-limbs in the same animal which we believe is a combination of natural fiber number variation between contralateral limbs.

INSERT FIGURE 3 HERE.

Continuous low frequency stimulation (CLFS) of the TA induced a reduction in fiber CSA, an increase in myonuclear content and changes in myosin heavy chain isoform composition.

As a model of endurance training, we applied CLFS to the TA unilaterally and used the contralateral leg as a control. To check that surgical intervention alone did not alter muscle mass, fiber CSA or myonuclear characteristics, sham IPGs and electrodes were implanted in the left hind-limb, and animals given 7 days to recover before euthanasia and muscle assessment. There were no significant differences in any characteristics studied between the operated and contralateral control TA in this sham group (Figure 4A-D). By contrast, 7 days of 24 hours per day 20Hz stimulation caused a

significant decrease in muscle mass (-12.6 ± 4.86%, *P* = 0.0026) (Figure 4A) in comparison to the unoperated control TA, concomitant with a similar decrease in muscle fiber CSA (-18.59 ± 11.41 %, *P* = 0.024), Figure 4B). Despite the loss in mass and fiber CSA, there was a highly variable yet significant increase in myonuclei per fiber (53.44 ± 44.87 %, *P* = 0.0328, Figure 4C) when assessed across the entire muscle cross-section, resulting in a significantly lower myonuclear domain size (-56.08 ± 27.87 %, *P* = 0.0097, Figure 4D).

When assessing fiber type-specific changes, there was a shift in fiber type proportion (Figure 4E-G) with a significant reduction in IIX/IIB fibers from 80.5 ± 8.4% to 62 ± 11.3%, *P* = 0.0003 after 7 days of CLFS. The percentage of type I (2.09 ± 1.6% vs. 4.95 ± 2.95%, *P* = 0.99) and IIA fibers (15.65 ± 6.75% vs. 15.53 ± 2.9%, *P* = 0.99) did not alter significantly between control and CLFS limbs respectively, although there was a substantial increase in Type I/IIA hybrids following CLFS (1.78 ± 1.8% to 17.52 ± 8.2%, *P* = 0.0032) suggesting that IIX/IIB fibers had shifted to IIA and existing IIA fibers had shifted to a type I/IIA hybrid phenotype. Interestingly, there were no significant differences in fiber CSA (Type I Control, 1357 ± 225μm^2 vs. Type I CLFS, 1252 ± 100μm^2, *P* = 0.99. Type I/IIA hybrid control 1201 ± 370μm^2 vs. Type I/IIA hybrid CLFS 1061 ± 160μm^2, *P* = 0.97. Type IIA Control 1370 ± 141μm^2 vs. Type IIA CLFS 1316 ± 157μm^2, *P* = 0.99. Type IIX/IIB control 2253 ± 371μm^2 vs. Type IIX/IIB CLFS 1954 ± 312μm^2, *P* = 0.45 (Figure 4H-J), despite the overall significant decrease in muscle fiber CSA (-18.59 ± 11.41%, *P* = 0.024). Therefore, the transformation of IIX/IIB to IIA myosin isoforms is probably the combined effect of insignificant decreases in fiber size, as well as a shift in fiber type proportion (Figure 4E-G).

To further elucidate the significant increase in myonuclei per fiber across the entire muscle cross-section following CLFS, we analysed myonuclei per fiber cross-section for each fiber type. While there were trends suggesting addition of myonuclei in Type I (0.88 ± 0.15 vs. 1.06 ± 0.16, *P* = 0.83, Figure 4K), Type I/IIA hybrid (0.94 ± 0.06 vs. 1.1 ± 0.16, *P* = 0.85, Supplementary Figure 3C), and Type IIA (0.94 ± 0.19 vs. 1.26 ± 0.23, *P* = 0.14, Figure 4L) fibers, the increase in the mean value only

reached significance in IIX/IIB fibers (0.85 ± 0.23 vs. 1.32 ± 0.31, *P* = 0.0044, Figure 4M). This was further reflected in the sizes of the myonuclear domain, which was significantly reduced only in the IIX/IIB fibers (3990 ± 2554μm^2 vs. 1232 ± 394 μm^2, *P* = 0.0007, Figure 4P).

INSERT FIGURE 4 HERE

Loaded resistance training (Spillover) produces a greater hypertrophic and myonuclear response than concentric resistance training.

Loaded RT produced a 3.3 ± 1.6% change in muscle mass after just 2 days of stimulation (*P* = 0.1) and reached statistical significance after 10 days (13.6 ± 5.8%, *P* = < 0.0001), 20 days (16.7 ± 4.4%, *P* = <0.0001) and 30 days (15.9 ± 5.6%, *P* = < 0.0001), in comparison to both sham surgery (*P* < 0.001) and their contralateral internal controls (*P* < 0.001) (Figure 5A). There were no significant differences between 10, 20 and 30 days of loaded RT, illustrating that muscle mass had plateaued between 10 and 20 days and thus, further daily training did not increase muscle mass. Thirty days of training with the identical daily activation but no active resistance from the plantar flexors produced a significant increase in muscle mass (6.2 ± 4.5%, *P* = 0.05), but was significantly lower than with 10, 20 or 30 days of loaded RT (*P* = 0.0493, *P* = 0.0036 and *P* = 0.0037, Figure 5A). Analysing overall changes in muscle fiber CSA revealed a delayed increase compared to muscle mass (Figure 5B), with a trend suggesting an increase in fiber CSA after 20 days vs the sham control group (7.61 ± 1.58%, *P* = 0.316), which reached significance after 30 days vs. the sham control group (17.55 ± 8.56%, *P* = <0.0001). Concentric RT did not cause a significant increase in fiber CSA vs the sham control group (5.19 ± 2.23%, *P*= 0.78), meaning that 30 days loaded RT showed significantly higher increases in CSA than 30 days of concentric RT (*P* = 0.0019). Part of the early increases in mass may be due to muscle swelling, and the lack of a plateau in the CSA data suggests that fiber hypertrophy is ongoing even after 30 days of loaded RT. Similarly, myonuclei per fiber cross-section did not significantly increase after 2 and 10 days but showed a trend to increase after 20 days (35.29 ± 21.18%, *P* = 0.1948, Figure

5C) and reached significance after 30 days of loaded RT (54.59 ± 42.64%, P = 0.0041), which was also significantly higher than the 30-day concentric RT group (11.89 ± 10.06%, P = 0.0255, Figure 5C).

After identifying significant increases in both muscle mass, fiber CSA and myonuclei per fiber cross-section after 30 days of loaded RT, but no significant changes in anything but muscle mass after 30 days of concentric RT, we sought to identify any potential fiber type-specific adaptations at the 30 days timepoint. There were no significant changes in fiber type proportion, but we note fiber-type specific changes in size in response to loaded and concentric RT modalities, despite identical activity patterns and activation of all fibers simultaneously during stimulation. 30 days of loaded RT produced a significant increase in type I fiber CSA above the control group (1507 ± 261μm^2 vs. 1105 ± 241μm^2, P = 0.0031), whereas 30 days of concentric RT was not significantly different between the control and 30-day loaded RT group. (1273 ± 73.9μm^2, P > 0.907), (Figure 5H). While fiber CSA seemed to be observably higher in some animals, large variation in the training groups meant there were no significant differences between Type I/IIA hybrid fibers between control (1149 ± 188μm^2) and both 30 days of loaded (1359 ± 307μm^2, P = 0.558), or 30 days of concentric RT (1302 ± 95μm^2, P = 0.9474, Supplementary Figure 4B). Although modest trends appeared, no significant differences were detected in Type IIA fibers between control fiber CSA (1392 ± 154μm^2), and both 30 days of loaded (1650 ± 265μm^2, P =0.236), or 30 days of concentric RT (1522 ± 135μm^2, P =0.984), (Figure 5I). By contrast, a robust increase in Type IIX/IIB fiber CSA was observed between the control and 30 days of loaded RT (2481 ± 222 vs. 2969 ± 268μm^2, P <0.0001), which was not observed after 30 days of concentric RT (2673 ± 176μm^2, P = 0.795, Figure 5J).

Myonuclei per fiber cross-section was significantly higher across all fiber types studied after 30 days of loaded RT vs control: Type I (1.43 ± 0.26 vs. 1.023 ± 0.16, P = 0.0078, Figure 5K); Type I/IIA hybrids (1.28 ± 0.35 vs. 0.93 ± 0.14, P = 0.023, Supplementary Figure 4C); Type IIA (1.5 ± 0.31 vs. 1.047 ± 0.17, P = 0.0015, Figure 5L); and Type IIX/IIB (1.448 ± 0.36 vs. 1.062 ±0.24, P = 0.0161, Figure 5M). By

contrast, with concentric training, we only observed modest trends suggesting that myonuclei were added after 30 days but none reached significance (Type I, 1.23 ± 0.16, P = 0.823. Type I/IIA Hybrids, 1.28 ± 0.18, P = 0.11. Type IIA, 1.31 ± 0.22, P = 0.46. Type IIX/IIB, 1.39 ± 0.21, P = 0.18), (Figure 5M-P). Despite this, there were no significant differences between myonuclei per fiber after 30 days loaded and 30 days concentric RT (Type I, P = 0.89. Type I/IIA Hybrids, P = 0.98 Type IIA, P = 0.93. Type IIX/IIB, P =0.98). Furthermore, there were no significant differences in myonuclear domain size across any of the fiber types investigated between the control and both loaded and concentric 30-day training groups (Figure 5N-P), suggesting that myonuclei were added in proportion to the increase in fiber CSA.

Using simple linear regression analysis to assess the relationships between measured variables across our timecourse of RT, we found significant positive correlations between percent changes in muscle mass and percent changes in fiber CSA (R^2 = 0.2324, P = <0.007) and myonuclei per fiber cross-section (R^2 = 0.1568, P = 0.0303, Figure 7A-B). The co-efficient of variation between percent changes in muscle mass and percent change in myonuclear domain size was not significant, (R^2 = 0.08682, P = 0.114, Figure 7C). Percent change in fiber CSA had a significant positive correlation with percent change in myonuclei per fiber cross-section (R^2 = 0.3826, P = 0.0003) and had a positive trend toward significance with the percent change in myonuclear domain size (R^2 = 0.1214, P = 0.0592, Figure 7D-E). As expected, the co-efficient of variation for percent change in myonuclear domain size and percent change in myonuclei per fiber cross-section reached significance (R^2 = 0.8137, P = <0.0001, Figure 7F).

INSERT FIGURE 5 HERE

TTX-induced skeletal muscle disuse atrophy causes a loss of myonuclei, and subsequent recovery of muscle mass is associated with substantial myonuclear addition.

INSERT FIGURE 6 HERE

As previously reported (29), exposure to TTX produced a progressive loss in TA muscle mass of -6.98 ± 2.5% at 3 days, -29.4 ± 5% at 7 days and -50.7 ± 2.9% after 14 days. The changes were significant at all time points vs. the sham operated group, -0.03 ± 2.5 ($P < 0.0001$), (Figure 6A). After 14 days of TTX exposure, followed by 7 days of recovery by habitual activity, muscle mass significantly recovered by 51.7% vs. 14 days of TTX exposure ($P < 0.001$). Seven days of recovery did not completely restore muscle mass, as muscle mass was still significantly lower than the sham group ($P < 0.001$), although muscle mass was not significantly different to the 7 days of TTX administration group (*P = 0.56)*, which suggests that the rate of loss over 7 days is similar to the rate of recovery. We made a completely new immunohistochemical analysis for this paper, cutting new sections from the same frozen muscles for analysis of whole muscle cross-sections with the updated MyoVision software. A trend was observed, suggesting a loss in detected fibers after 14 days atrophy of -19.5 ± 7.8%, (P=0.052). However, when fiber number was manually counted on hematoxylin and eosin (H&E) stained tissue sections from 14-day TTX treatment, looking specifically at the most severely atrophied fibers, there was good agreement with the automatic detection in the most challenging fields of view, (87.7 ± 4.3%), where ~13% of the fibers had become too small or squashed to be successfully identified by MyoVision as a muscle fiber as opposed to interstitial tissue. With MyoVision 2.0, we added a feature for users to change the myofiber identification parameters in relation to circularity, solidity, and eccentricity to allow for adjustment to muscle phenotypes where cross-sectioned fibers become less round (more pennate architecture) and may be not identified based on default parameters (Supplementary Figure 2). However, for our analyses we kept the default parameters the same for consistency across experimental groups (0.6 circularity, 0.85 solidity, 0.95 eccentricity).

H&E staining showed no evidence of fiber loss, splitting or newly formed fibers in any of our multiple endpoints as previously reported (29, 30). Muscle fiber CSA progressively declined vs. the sham operated group, reaching significance at 7 days (-33.7 ± 9.2%, $P < 0.0001$) and further declining at 14 days (-53.7 ± 10.8%, ($P < 0.0001$). After cessation of TTX delivery and 7 days recovery, muscle fiber

CSA was still significantly lower than the sham operated group (P = 0.012), despite significantly increasing (-20.4 ± 11.1%) vs. the 14-day atrophy timepoint. Much like muscle mass, fiber CSA losses were not significantly different to the 7 days atrophy timepoint (P = 0.293), suggesting CSA recovered at the same rate as CSA loss (Figure 6B).

Measurements of myonuclei per fiber cross-sectional area revealed a trend suggesting myonuclei were being progressively lost after only 7 days of atrophy (-26.2 ± 21%, P = 0.45), later reaching significance after 14 days of atrophy (-40.72 ± 21%, P = 0.0489). From the substantial loss of myonuclei per fiber cross-section observed after 14 days of atrophy (-40.72 ± 21%), 7 days of recovery allowed for myonuclei per fiber cross-section to significantly increase by 38.67 ± 33.08% vs. their internal contralateral controls (P= 0.049). This suggests that myonuclei are added in substantial numbers above baseline values to aid in the regrowth of muscle following atrophy, (Figure 6C). Myonuclear domain size % changes did not differ significantly between any of the time points, (Figure 6D).

To identify whether the changes in myonuclear content varied between fiber types, we conducted further analyses on the 14-day atrophy group and 14-day atrophy with 7 days recovery group. Analysis of fiber type proportions at both timepoints revealed no significant differences in overall fiber type percentage, though a trend was observed for an increase in type IIA fibers after 14 days of atrophy (32.72 ± 8.07%, P = 0.357) and 14 days of atrophy with 7 days recovery (34 ± 12.04%, P = 0.118) vs. the control limbs (24.43 ± 6.12%), (Figure 6E-G). This was concomitant with trends suggesting a reduction in type IIX/IIB fibers after 14 days atrophy (60.86 ± 10.14%, P = 0.2153), and following subsequent recovery (59.04 ± 13.44%, P = 0.0575) versus the control group (70.01 ± 6.19%) (Figure 6G).

With no clear shifts in fiber type, we assessed fiber CSA to determine whether atrophy was similar across fiber types. The shape of the bar charts looks similar for each fiber type, but significant

differences were only noted in type IIA and IIX/B fibers. In comparison to the control type I fibers (1179 ± 178μm^2), 14 days of TTX treatment did not cause a significant decrease in fiber CSA (796 ± 170μm^2, *P* = 0.14), nor a significant change in the recovery group (988 ± 155μm^2), from either the control (*P* = 0.94), or atrophied muscles (*P* = 0.98, Figure 6H). Similarly, type I/IIA hybrids (1148 ± 130μm^2) showed no significant decline following atrophy (796 ± 125μm^2, *P* = 0.24), or recovery from atrophy (1009 ± 72μm^2, *P* = 0.957, Supplementary Figure 5B). However, there was a significant decrease in type IIA fiber CSA after 14 days (1423 ± 298μm^2 vs. 968 ± 89μm^2, *P* = 0.035), which had recovered back to the mean control CSA after recovery (1368 ± 77μm^2, P = 0.99, Figure 6I). By contrast, while type IIX/IIB fiber CSA was reduced by 56.6% in the atrophy group (2325 ± 394μm^2 vs. 1010 ± 228μm^2, *P* <0.0001), fiber CSA was not able to recover completely to the level of the control muscle after 7 days of recovery (1746 ± 601μm^2, *P* = 0.0016), although this was significantly higher than the 14 days of atrophy timepoint (*P* = <0.0001, Figure 6J).

Assessment of myonuclei per fiber cross-section in type I fibers revealed no differences between the control TA (0.93 ± 0.25) and the 14-day atrophy group (1.11 ± 0.24, *P* = 0.96), or the 14-day atrophy with 7 days of recovery group (0.86 ± 0.29, *P* = 0.99), (Figure 6K). Myonuclei per fiber cross-section in type I/IIA hybrid fibers revealed a significant reduction in myonuclei (1.16 ± 0.24 vs. 0.71 ± 0.17, *P* = 0.0219), but recovered back to control levels after just 7 days (1.23 ± 0.31, *P* = 0.99), and was significantly higher than the 14-day atrophy timepoint (*P* = 0.0239) for this fiber type (Supplementary Figure 5C). A similar trend was observed in type IIA fibers which lost myonuclei after 14 days of atrophy (1.2 ± 0.26 vs. 0.68 ± 0.26, *P* = 0.0046), but recovered after 7 days (1.16 ± 0.3, *P* = 0.05) to the extent that there was no significant difference from the control group (*P* = 0.99), (Figure 6L). While myonuclei number in the type IIX/IIB fiber was significantly reduced after the atrophy period compared to the control group (1.09 ± 0.18 vs. 0.61 ± 0.08, *P* = 0.01), myonuclei number per fiber cross-section significantly increased in the recovery group (1.68 ± 0.34), both above the 14 days atrophy group (*P* = <0.0001) and surprisingly further beyond the control group (*P* = 0.0005), (Figure

6M). We then assessed whether the myonuclear domain size was therefore altered following substantial atrophy and found no significant differences in type I (P >0.3), type I/IIA hybrid (P >0.98), or type IIA (P >0.90) fibers, between the control, atrophy, and atrophy with recovery groups, (Figure 6N-P). However, a trend was detected in type IIX/IIB fibers, suggesting a decrease in domain size between the control and 14-day atrophy group (2232 ± 731μm^2 vs. 1664 ± 310μm^2, P = 0.285). A significantly lower myonuclear domain size was detected between the control TAs and the 14-day atrophy with 7-day recovery group (970 ± 241μm^2, P <0.0001), (Figure 6P).

Linear regression analysis revealed a significant positive correlation between percent change in muscle mass and percent change in fiber CSA (R^2 = 0.8589, P = <0.0001), percent change in myonuclei per fiber cross-section (R^2 = 0.8589, P = <0.0001) and percent change in myonuclear domain size (R^2 = 0.4550, P = 0.0008, Figure 7G-I). There were also significant positive correlations between percent change in fiber CSA and both percent change in myonuclei per fiber cross-section (R^2 = 0.8079, P = <0.0001) and percent change in myonuclear domain size (R^2 = 0.5439, P = 0.0001, Figure 7J-K). The co-efficient of variation between the percent change in myonuclei per fiber cross-section and percent change in myonuclear domain size was also significant (R^2 = 0.2468, P = 0.022, Figure 7L).

Discussion:

In both developing and adult mammalian skeletal muscle, myonuclei number, often referred to as DNA content, varies with muscle fiber size although this relationship is not completely linear, nor is it fully understood in all contexts of muscle plasticity (7, 24, 35). Our objective was to understand the fiber type specific changes in cross-sectional area and whether this correlated with changes in myonuclear content in our models of growth, endurance training, atrophy and recovery. We developed MyoVision as the first unbiased, fully automatic software that is freely available to the muscle research community, and since then, there has been significant interest in such analytical

556 packages for muscle cross-sections (36-41). Despite the overall interest, MyoVision remains one of
557 only two freely available programs that include myonuclear quantification and the only one for
558 which this function is validated. A major limitation of MyoVision was its computational inefficiency
559 that precluded analysis of large cross-sections, such as the whole rat TA, taken at high magnification.
560 In most instances, the previous version of the software would not successfully analyse such large
561 images, but the new software provides this capability through improved computational speed and
562 efficiency. Additionally, MyoVision analysis was previously sensitive to background noise, which
563 increased the requirement on microscope image quality. To address these shortcomings, we have
564 updated MyoVision and optimized the software to allow for rapid and unsupervised quantification of
565 hundreds of thousands of individual myofibers and millions of nuclei on histological cross-sections
566 (www.myoanalytics.com/myovision2).

567 CLFS for 7 days which mimics endurance training caused a significant reduction in mean muscle mass
568 (-12.6 ± 4.9%, P = 0.0026), mean fiber CSA (-18.6 ± 11.4 %, P = 0.024) and a shift from glycolytic to
569 smaller, more oxidative fibers (type IIX/IIB fiber percentage fell from 81% to 62%). There were no
570 changes in fiber CSA when assessed at the fiber type level (Figure 4H-J), suggesting that the larger
571 IIX/IIB fibers that shifted myosin heavy chain content also reduced their fiber area which may be an
572 adaptation to reduce the diffusion distance to allow increased respiratory gas exchange associated
573 with a shift to oxidative metabolism (42-46). Myonuclear addition is generally considered to be a
574 feature of resistance exercise-induced hypertrophy, as a mechanism to support both repair of
575 damaged muscle fibers unaccustomed to exercise (4, 47) and to support transcription across a larger
576 area of cytoplasm (35, 48, 49). However, we found significant increases in myonuclei per fiber cross-
577 section especially in type IIX/IIB glycolytic fibers in response to CLFS. As mean fiber area did not
578 change, IIX/IIB myofiber cytoplasm became hypernucleated per fiber cross-section, so that there was
579 a significant reduction in myonuclear domain size (-69%, P = 0.0007), which was closer to the value
580 for oxidative fibers in control muscle.

We then studied the fiber type specific effects of RT using spillover (loaded) contractions and high-frequency concentric contractions. While loading from the antagonistic muscle group differs between our RT modalities, our model avoids the complication of variable recruitment among fiber types during the exercise intervention. This allowed us to directly compare the differences in loading on fiber type specific adaptations so that the total volume of activation can be excluded as a factor for differences between fiber types in terms of exercise induced myonuclear accretion. Thirty days of loaded RT caused significantly larger increases in muscle mass, fiber CSA and myonuclear accretion than 30 days of concentric RT, similarly to Eftestøl and colleagues who used a non-surgical model to exercise rat dorsiflexor muscles using transcutaneous electrical stimulation with external load applied through the use of a resisting footplate (50). They reported that higher load was associated with greater fiber hypertrophy and greater myonuclear accretion but did not assess fiber type specific effects. In our loaded RT model after 30 days, fiber area increased significantly in type I fibers by a mean of 36% (Figure 5H) and by a mean of only 19% in type IIX/IIB fibers (Figure 5J). While this increase is somewhat larger in the slow muscle fibers, the relatively small proportion of type I fibers (<6%) and large proportion of IIX/IIB fibers means that IIX/IIB contribute more to whole muscle fiber hypertrophy. However, this is an interesting observation of the potential functional significance of hypertrophy of small populations of slow fibers in a predominantly fast twitch muscle during hypertrophy. Furthermore, myonuclear accretion was similar across all fiber types (Figure 5K-M), suggesting that the accretion of myonuclei is strongly associated with load and activity in this instance. It has previously been argued that slower fibers are more susceptible to exercise-induced damage but this can often be explained by their greater activation in voluntary movement, being recruited to a larger extent than fast oxidative and fast glycolytic fibers (51, 52). Despite this, a recent study in mice using a voluntary exercise on a high load resistance wheel, produced myonuclear accretion in a load dependent manner in the plantarflexor muscles of mice, and the addition of myonuclei occurred similarly across all fiber types (53). In contrast, progressive weighted wheel running (PoWeR) in mice results in both fiber type-specific and fiber type-independent

607 adaptations that differ based on the muscle studied (4). This probably reflects differences in
608 activation and load during voluntary exercise, as well as early damage-related fusion of satellite cells
609 which has previously been reported after unaccustomed exercise (47, 54, 55).

610 Myonuclear loss or maintenance during muscle disuse is of particular interest since the signals
611 related to exercise and load are reduced. Previously, the relationship between muscle loss during
612 disuse in rodents has been performed using injury to the nerve/denervation (25, 56, 57) and hind-
613 limb unloading (22, 58, 59), although the latter model does not control for motor activity, and in
614 some instances it can even be increased, while the load is reduced (60, 61). The use of TTX to study
615 muscle atrophy has been less widely adopted (25, 29, 62, 63). However, TTX nerve treatment causes
616 muscle atrophy through prevention of generation or propagation of action potentials in the nerve,
617 without axonal damage so disuse can be followed by a period of recovery. Trophic factors
618 dependent on axon integrity may continue to have influence on their associated muscle fibers, while
619 substantial sarcoplasm is lost within the muscle fibers (29, 64, 65).

620 As we have previously reported (29), onset of TTX treatment causes a progressive loss in muscle
621 mass and mean fiber CSA reaching significance after 7 days and further declining at 14 days (Figure
622 6A-B). Our new fiber-type specific analysis shows that this is mainly attributed to significant loss of
623 CSA in type IIA (-47%) and IIX/IIB fibers (-56%) (Figure 6I-J) while simultaneously reducing myonuclei
624 per fiber cross-section in both IIA and IIX/IIB fibers (43%), therefore maintaining myonuclear domain
625 size. Intriguingly, type I fibers did not atrophy significantly, and they maintained their myonuclei
626 number. Similar treatment involving the entire sciatic nerve for 2 weeks found that type IIA muscle
627 fibers atrophied less (29%) than type IIB fibers (43%) in the TA of rats (63). Sciatic nerve block also
628 prevents activity of the plantarflexors; it was observed that the lateral gastrocnemius IIB and IIA
629 fibers showed less atrophy (23-26%) than the resident type I fibers (44%), but in the soleus, both fast
630 and slow fibers atrophied to the same extent (39% versus 43%). Differences in the rates and total
631 extent of muscle atrophy have been reported between different muscles and different fiber types

which may be related to oxidative capacity, protein synthetic/degradation rates and the resting length of the muscle (63, 66, 67). Only one study to our knowledge has measured myonuclei number in response to TTX treatment, although this was performed in mice. Intravital imaging showed no decrease in myonuclei with intravital imaging after 3 weeks in the EDL muscle which may be related to species differences or the fact that the EDL crosses two joints and therefore has a higher level of passive tension, perhaps enough to prevent loss of myonuclei.

During the 7-days recovery post TTX treatment, muscle mass significantly recovered by 51.7% versus 14 days of TTX exposure ($P < 0.001$). Type IIA fibers recovered fiber CSA and myonuclei per fiber cross-section measurements in line with control levels during this period. This recovery was not matched in the less oxidative type IIX/IIB fibers which had only partially recovered their CSA from 14 days of nerve silencing ($P = 0.003$). Remarkably, myonuclei per fiber cross-section was higher in comparison to both the atrophied muscle ($P = <0.0001$) and the control muscle ($P = 0.0005$) in IIX/IIB fibers, suggesting that myonuclear populations did not only recover back to the point of baseline, but were also added past homeostatic levels to support the substantial recovery of muscle mass and fiber CSA from severe atrophy, somewhat like resistance exercise-induced myonuclear accretion. This resulted in hypernucleated type IIX/IIB fibers, versus their control counterparts. We also observed this characteristic in our CLFS model, suggesting that due to type IIX/IIB fibers having larger myonuclear domains than their slower, more oxidative counterparts under control conditions, they may be more dependent on myonuclear accretion to support the changes in activity or periods of regrowth. It is of significant interest whether type IIX/IIB fibers retain the extra myonuclei added during the recovery from TTX-induced atrophy or whether they are lost as muscle returns to basal mass, so that they act as 'temporary' myonuclei to support the rapid growth. Or, if they are retained how this would affect subsequent periods of unloading and future periods of growth.

Future Considerations:

The use of IPGs allows for programming and control over both endurance and resistance exercise so that training duration, contraction modality, repetitions, sets, rest and the timing of exercise within the circadian cycle can all be prescribed. IPGs can be easily programmed to switch on or off allowing for periods of detraining and subsequent retraining with minimal intervention or use of supraphysiological methods. Analogously, the careful planning and loading of osmotic pumps to deliver TTX to a motor nerve allows for periods of disuse induced atrophy and subsequent recovery. The replacement of the osmotic pump or use of programmable infusion pumps would also allow for continuous cycling of nerve block and recovery to simulate repeated bed rest in humans. Further functions are continually being added to the automated image analysis program, MyoVision www.myoanalytics.com/myovision2, including guidance on supported image file types and minimum recommended computer requirements.

Conclusion:

We propose that the number of myonuclei is not fixed, probably reflects the changes in activity requirements of the muscle fiber and does not always correlate with fiber size. The myonuclear domain appears highly flexible and adaptations often differ by fiber type. High load RT resulted in increased muscle size associated with higher myonuclear content per muscle fiber, whereas low-load continuous stimulation increased myonuclear content but reduced muscle fiber size. TTX-induced nerve silencing caused atrophy and myonuclear loss, but both were restored with recovery of activity. The recovery in type IIX/IIB fibers includes an over compensatory addition of myonuclei to the muscle fiber. Overall, our models of high load short duration and low load continuous stimulation, and recovery after disuse all resulted in substantial increases in myonuclei without histological signs of muscle damage as assessed by histology.

Supplementary Figures 1-5

https://doi.org/10.6084/m9.figshare.17904347 (Supplementary File 1, Supplementary Figures 1-2).

https://doi.org/10.6084/m9.figshare.16775677 (Supplementary File 2, Supplementary Figures 3-5).

Acknowledgments:

The authors thank Dr Hazel Sutherland for expert help with the implant operations and muscle harvesting.

The authors thank Dr. Kevin Murach for his discussions and useful insights on the manuscript.

Author Contributions:

M.V, J.C.J designed experiments. M.V, J.C.J performed experiments. Y.W and M.V analyzed and interpreted data. Y.W. built the updated software. M.V and Y.W. wrote the manuscript and prepared figures with the support and review of J.C.J and C.A.P.

Declaration of interests:

In the past year, Y.W. has worked as a consultant for the Core Muscle Research laboratory at the University of Alabama and he declares ownership in MyoAnalytics, LLC.

References:

1. **Schiaffino S, Dyar KA, Ciciliot S, Blaauw B, and Sandri M**. Mechanisms regulating skeletal muscle growth and atrophy. *The FEBS journal* 280: 4294-4314, 2013.
2. **Sharples AP, Polydorou I, Hughes DC, Owens DJ, Hughes TM, and Stewart CE**. Skeletal muscle cells possess a 'memory'of acute early life TNF-α exposure: role of epigenetic adaptation. *Biogerontology* 17: 603-617, 2016.
3. **Seaborne R, Strauss J, Cocks M, Shepherd S, O'Brien T, Van Someren K, Bell P, Murgatroyd C, Morton J, and Stewart C**. Methylome of human skeletal muscle after acute & chronic resistance exercise training, detraining & retraining. *Scientific data* 5: 1-9, 2018.
4. **Murach KA, Mobley CB, Zdunek CJ, Frick KK, Jones SR, McCarthy JJ, Peterson CA, and Dungan CM**. Muscle memory: myonuclear accretion, maintenance, morphology, and miRNA levels with training and detraining in adult mice. *Journal of cachexia, sarcopenia and muscle* 2020.
5. **Gundersen K**. Muscle memory and a new cellular model for muscle atrophy and hypertrophy. *Journal of Experimental Biology* 219: 235-242, 2016.
6. **Joplin R, Franchi L, and Salmons S**. Changes in the size and synthetic activity of nuclear populations in chronically stimulated rabbit skeletal muscle. *Journal of anatomy* 155: 39, 1987.
7. **Cramer AA, Prasad V, Eftestøl E, Song T, Hansson K-A, Dugdale HF, Sadayappan S, Ochala J, Gundersen K, and Millay DP**. Nuclear numbers in syncytial muscle fibers promote size but limit the development of larger myonuclear domains. *Nature communications* 11: 1-14, 2020.

8. **Kirby TJ, Patel RM, McClintock TS, Dupont-Versteegden EE, Peterson CA, and McCarthy JJ**. Myonuclear transcription is responsive to mechanical load and DNA content but uncoupled from cell size during hypertrophy. *Molecular biology of the cell* 27: 788-798, 2016.
9. **Windner SE, Manhart A, Brown A, Mogilner A, and Baylies MK**. Nuclear scaling is coordinated among individual nuclei in multinucleated muscle fibers. *Developmental Cell* 49: 48-62. e43, 2019.
10. **Goldspink DF, Cox VM, Smith SK, Eaves LA, Osbaldeston NJ, Lee DM, and Mantle D**. Muscle growth in response to mechanical stimuli. *American Journal of Physiology-Endocrinology And Metabolism* 268: E288-E297, 1995.
11. **Nader GA, McLoughlin TJ, and Esser KA**. mTOR function in skeletal muscle hypertrophy: increased ribosomal RNA via cell cycle regulators. *American Journal of Physiology-Cell Physiology* 2005.
12. **McCarthy JJ, Mula J, Miyazaki M, Erfani R, Garrison K, Farooqui AB, Srikuea R, Lawson BA, Grimes B, and Keller C**. Effective fiber hypertrophy in satellite cell-depleted skeletal muscle. *Development* 138: 3657-3666, 2011.
13. **Englund DA, Peck BD, Murach KA, Neal AC, Caldwell HA, McCarthy JJ, Peterson CA, and Dupont-Versteegden EE**. Resident muscle stem cells are not required for testosterone-induced skeletal muscle hypertrophy. *American Journal of Physiology-Cell Physiology* 317: C719-C724, 2019.
14. **Murach KA, White SH, Wen Y, Ho A, Dupont-Versteegden EE, McCarthy JJ, and Peterson CA**. Differential requirement for satellite cells during overload-induced muscle hypertrophy in growing versus mature mice. *Skeletal muscle* 7: 1-13, 2017.
15. **Goh Q, Song T, Petrany MJ, Cramer AA, Sun C, Sadayappan S, Lee S-J, and Millay DP**. Myonuclear accretion is a determinant of exercise-induced remodeling in skeletal muscle. *Elife* 8: e44876, 2019.
16. **Englund DA, Murach KA, Dungan CM, Figueiredo VC, Vechetti Jr IJ, Dupont-Versteegden EE, McCarthy JJ, and Peterson CA**. Depletion of resident muscle stem cells negatively impacts running volume, physical function and muscle hypertrophy in response to lifelong physical activity. *American Journal of Physiology-Cell Physiology* 2020.
17. **Englund DA, Figueiredo VC, Dungan CM, Murach KA, Peck BD, Petrosino JM, Brightwell CR, Dupont AM, Neal AC, and Fry CS**. Satellite cell depletion disrupts transcriptional coordination and muscle adaptation to exercise. *Function* 2: zqaa033, 2021.
18. **Verma M, Asakura Y, Murakonda BSR, Pengo T, Latroche C, Chazaud B, McLoon LK, and Asakura A**. Muscle satellite cell cross-talk with a vascular niche maintains quiescence via VEGF and notch signaling. *Cell stem cell* 23: 530-543. e539, 2018.
19. **Madaro L, Mozzetta C, Biferali B, and Proietti D**. Fibro-Adipogenic Progenitors (FAPs) cross-talk in skeletal muscle: the social network. *Frontiers in physiology* 10: 1074, 2019.
20. **Murach KA, Vechetti Jr IJ, Van Pelt DW, Crow SE, Dungan CM, Figueiredo VC, Kosmac K, Fu X, Richards CI, and Fry CS**. Fusion-independent satellite cell communication to muscle fibers during load-induced hypertrophy. *Function* 1: zqaa009, 2020.
21. **Murach KA, Peck BD, Policastro RA, Vechetti IJ, Van Pelt DW, Dungan CM, Denes LT, Fu X, Brightwell CR, and Zentner GE**. Early satellite cell communication creates a permissive environment for long-term muscle growth. *Iscience* 24: 102372, 2021.
22. **Dupont-Versteegden EE, Strotman BA, Gurley CM, Gaddy D, Knox M, Fluckey JD, and Peterson CA**. Nuclear translocation of EndoG at the initiation of disuse muscle atrophy and apoptosis is specific to myonuclei. *Am J Physiol Regul Integr Comp Physiol* 291: R1730-1740, 2006.
23. **Dungan CM, Murach KA, Frick KK, Jones SR, Crow SE, Englund DA, Vechetti Jr IJ, Figueiredo VC, Levitan BM, and Satin J**. Elevated myonuclear density during skeletal muscle hypertrophy in response to training is reversed during detraining. *American Journal of Physiology-Cell Physiology* 316: C649-C654, 2019.
24. **Snijders T, Aussieker T, Holwerda A, Parise G, van Loon LJ, and Verdijk LB**. The concept of skeletal muscle memory: Evidence from animal and human studies. *Acta Physiologica* e13465, 2020.

762 25. **Bruusgaard JC, and Gundersen K**. In vivo time-lapse microscopy reveals no loss of murine
763 myonuclei during weeks of muscle atrophy. *The Journal of clinical investigation* 118: 1450-1457,
764 2008.
765 26. **Stewart MD, Jang CW, Hong NW, Austin AP, and Behringer RR**. Dual fluorescent protein
766 reporters for studying cell behaviors in vivo. *genesis* 47: 708-717, 2009.
767 27. **Hastings RL, Massopust RT, Haddix SG, Lee Yi, and Thompson WJ**. Exclusive vital labeling of
768 myonuclei for studying myonuclear arrangement in mouse skeletal muscle tissue. *Skeletal Muscle*
769 10: 1-13, 2020.
770 28. **Hansson K-A, Eftestøl E, Bruusgaard JC, Juvkam I, Cramer AW, Malthe-Sørenssen A, Millay**
771 **DP, and Gundersen K**. Myonuclear content regulates cell size with similar scaling properties in mice
772 and humans. *Nature communications* 11: 1-14, 2020.
773 29. **Fisher AG, Seaborne RA, Hughes TM, Gutteridge A, Stewart C, Coulson JM, Sharples AP,**
774 **and Jarvis JC**. Transcriptomic and epigenetic regulation of disuse atrophy and the return to activity in
775 skeletal muscle. *The Faseb Journal* 31: 5268-5282, 2017.
776 30. **Schmoll M, Unger E, Sutherland H, Haller M, Bijak M, Lanmüller H, and Jarvis JC**. SpillOver
777 stimulation: A novel hypertrophy model using co-contraction of the plantar-flexors to load the tibial
778 anterior muscle in rats. *PLOS ONE* 13: e0207886, 2018.
779 31. **Jarvis J, and Salmons S**. A family of neuromuscular stimulators with optical transcutaneous
780 control. *Journal of medical engineering & technology* 15: 53-57, 1991.
781 32. **Jarvis JC**. Power production and working capacity of rabbit tibialis anterior muscles after
782 chronic electrical stimulation at 10 Hz. *The Journal of Physiology* 470: 157-169, 1993.
783 33. **Wen Y, Murach KA, Vechetti Jr IJ, Fry CS, Vickery C, Peterson CA, McCarthy JJ, and**
784 **Campbell KS**. MyoVision: software for automated high-content analysis of skeletal muscle
785 immunohistochemistry. *Journal of Applied Physiology* 124: 40-51, 2018.
786 34. **Ronneberger O, Fischer P, and Brox T**. U-net: Convolutional networks for biomedical image
787 segmentation. In: *International Conference on Medical image computing and computer-assisted*
788 *intervention*Springer, 2015, p. 234-241.
789 35. **Karlsen A, Couppé C, Andersen JL, Mikkelsen UR, Nielsen RH, Magnusson SP, Kjaer M, and**
790 **Mackey AL**. Matters of fiber size and myonuclear domain: does size matter more than age? *Muscle*
791 *& nerve* 52: 1040-1046, 2015.
792 36. **Mayeuf-Louchart A, Hardy D, Thorel Q, Roux P, Gueniot L, Briand D, Mazeraud A, Bouglé A,**
793 **Shorte SL, and Staels B**. MuscleJ: a high-content analysis method to study skeletal muscle with a
794 new Fiji tool. *Skeletal muscle* 8: 1-11, 2018.
795 37. **Encarnacion-Rivera L, Foltz S, Hartzell HC, and Choo H**. Myosoft: an automated muscle
796 histology analysis tool using machine learning algorithm utilizing FIJI/ImageJ software. *PloS one* 15:
797 e0229041, 2020.
798 38. **Lau YS, Xu L, Gao Y, and Han R**. Automated muscle histopathology analysis using CellProfiler.
799 *Skeletal muscle* 8: 1-9, 2018.
800 39. **Waisman A, Norris AM, Costa ME, and Kopinke D**. Automatic and unbiased segmentation
801 and quantification of myofibers in skeletal muscle. *Scientific Reports* 11: 1-14, 2021.
802 40. **Kastenschmidt JM, Ellefsen KL, Mannaa AH, Giebel JJ, Yahia R, Ayer RE, Pham P, Rios R,**
803 **Vetrone SA, and Mozaffar T**. QuantiMus: a machine learning-based approach for high precision
804 analysis of skeletal muscle morphology. *Frontiers in physiology* 10: 1416, 2019.
805 41. **Sertel O, Dogdas B, Chiu CS, and Gurcan MN**. Microscopic image analysis for quantitative
806 characterization of muscle fiber type composition. *Computerized Medical Imaging and Graphics* 35:
807 616-628, 2011.
808 42. **Brown MD, Cotter MA, Hudlická O, and Vrbová G**. The effects of different patterns of
809 muscle activity on capillary density, mechanical properties and structure of slow and fast rabbit
810 muscles. *Pflügers Archiv* 361: 241-250, 1976.

43. **Egginton S, and Hudlicka O**. Early changes in performance, blood flow and capillary fine structure in rat fast muscles induced by electrical stimulation. *The Journal of physiology* 515: 265-275, 1999.
44. **Hudlicka O, Brown M, Cotter M, Smith M, and Vrbova G**. The effect of long-term stimulation of fast muscles on their blood flow, metabolism and ability to withstand fatigue. *Pflügers Archiv* 369: 141-149, 1977.
45. **Hudlicka O, Dodd L, Renkin E, and Gray S**. Early changes in fiber profile and capillary density in long-term stimulated muscles. *American Journal of Physiology-Heart and Circulatory Physiology* 243: H528-H535, 1982.
46. **Hudlická O, Egginton S, and Brown M**. Capillary diffusion distances-their importance for cardiac and skeletal muscle performance. *Physiology* 3: 134-138, 1988.
47. **Mackey AL, and Kjaer M**. The breaking and making of healthy adult human skeletal muscle in vivo. *Skeletal muscle* 7: 24, 2017.
48. **Karlsen A, Soendenbroe C, Malmgaard-Clausen NM, Wagener F, Moeller CE, Senhaji Z, Damberg K, Andersen JL, Schjerling P, and Kjaer M**. Preserved capacity for satellite cell proliferation, regeneration, and hypertrophy in the skeletal muscle of healthy elderly men. *The FASEB Journal* 34: 6418-6436, 2020.
49. **Snijders T, Holwerda AM, van Loon LJ, and Verdijk LB**. Myonuclear content and domain size in small versus larger muscle fibres in response to 12 weeks of resistance exercise training in older adults. *Acta Physiologica* e13599, 2020.
50. **Eftestøl E, Egner IM, Lunde IG, Ellefsen S, Andersen T, Sjåland C, Gundersen K, and Bruusgaard JC**. Increased hypertrophic response with increased mechanical load in skeletal muscles receiving identical activity patterns. *American Journal of Physiology-Cell Physiology* 311: C616-C629, 2016.
51. **Vijayan K, Thompson JL, and Riley DA**. Sarcomere lesion damage occurs mainly in slow fibers of reloaded rat adductor longus muscles. *Journal of Applied Physiology* 85: 1017-1023, 1998.
52. **Vijayan K, Thompson JL, Norenberg KM, Fitts R, and Riley DA**. Fiber-type susceptibility to eccentric contraction-induced damage of hindlimb-unloaded rat AL muscles. *Journal of Applied Physiology* 90: 770-776, 2001.
53. **Masschelein E, D'Hulst G, Zvick J, Hinte L, Soro-Arnaiz I, Gorski T, von Meyenn F, Bar-Nur O, and De Bock K**. Exercise promotes satellite cell contribution to myofibers in a load-dependent manner. *Skeletal Muscle* 10: 21, 2020.
54. **Smith HK, Maxwell L, Rodgers CD, McKee NH, and Plyley MJ**. Exercise-enhanced satellite cell proliferation and new myonuclear accretion in rat skeletal muscle. *Journal of Applied Physiology* 90: 1407-1414, 2001.
55. **Crameri R, Aagaard P, Qvortrup K, Langberg H, Olesen J, and Kjær M**. Myofibre damage in human skeletal muscle: effects of electrical stimulation versus voluntary contraction. *The Journal of physiology* 583: 365-380, 2007.
56. **Ashley Z, Salmons S, Boncompagni S, Protasi F, Russold M, Lanmuller H, Mayr W, Sutherland H, and Jarvis JC**. Effects of chronic electrical stimulation on long-term denervated muscles of the rabbit hind limb. *Journal of Muscle Research and Cell Motility* 28: 203-217, 2007.
57. **Ashley Z, Sutherland H, Lanmuller H, Russold M, Unger E, Bijak M, Mayr W, Boncompagni S, Protasi F, and Salmons S**. Atrophy, but not necrosis, in rabbit skeletal muscle denervated for periods up to one year. *American Journal of Physiology-Cell Physiology* 292: C440-C451, 2007.
58. **Jackson JR, Mula J, Kirby TJ, Fry CS, Lee JD, Ubele MF, Campbell KS, McCarthy JJ, Peterson CA, and Dupont-Versteegden EE**. Satellite cell depletion does not inhibit adult skeletal muscle regrowth following unloading-induced atrophy. *American Journal of Physiology-Cell Physiology* 2012.
59. **Seaborne RA, Hughes DC, Turner DC, Owens DJ, Baehr LM, Gorski P, Semenova EA, Borisov OV, Larin AK, and Popov DV**. UBR5 is a novel E3 ubiquitin ligase involved in skeletal muscle hypertrophy and recovery from atrophy. *The Journal of physiology* 597: 3727-3749, 2019.

60. **Michel RN, and Gardiner PF**. To what extent is hindlimb suspension a model of disuse? *Muscle & Nerve: Official Journal of the American Association of Electrodiagnostic Medicine* 13: 646-653, 1990.
61. **Pierotti DJ, Roy RR, Flores V, and Edgerton V**. Influence of 7 days of hindlimb suspension and intermittent weight support on rat muscle mechanical properties. *Aviation, space, and environmental medicine* 61: 205-210, 1990.
62. **Cormery B, Pons F, Marini J-F, and Gardiner PF**. Myosin heavy chains in fibers of TTX-paralyzed rat soleus and medial gastrocnemius muscles. *Journal of Applied Physiology* 88: 66-76, 2000.
63. **Salter A-CD, Richmond FJ, and Loeb GE**. Effects of muscle immobilization at different lengths on tetrodotoxin-induced disuse atrophy. *IEEE Transactions on neural systems and rehabilitation engineering* 11: 209-217, 2003.
64. **Martinov VN, and Njå A**. A microcapsule technique for long-term conduction block of the sciatic nerve by tetrodotoxin. *Journal of neuroscience methods* 141: 199-205, 2005.
65. **Reid B, Martinov VN, Njå A, Lømo T, and Bewick GS**. Activity-dependent plasticity of transmitter release from nerve terminals in rat fast and slow muscles. *Journal of Neuroscience* 23: 9340-9348, 2003.
66. **Baehr LM, West DW, Marcotte G, Marshall AG, De Sousa LG, Baar K, and Bodine SC**. Age-related deficits in skeletal muscle recovery following disuse are associated with neuromuscular junction instability and ER stress, not impaired protein synthesis. *Aging (Albany NY)* 8: 127, 2016.
67. **Baehr LM, West DW, Marshall AG, Marcotte GR, Baar K, and Bodine SC**. Muscle-specific and age-related changes in protein synthesis and protein degradation in response to hindlimb unloading in rats. *Journal of applied physiology* 122: 1336-1350, 2017.

885 Figure Legends:

886 Figure 1: Schematic representation of electrical stimulation experimental time courses studied and timepoints of
887 euthanasia and muscle harvest. For electrical stimulation experiments, an implantable pulse generator (IPG) was placed
888 within the abdomen with electrodes leading subcutaneously to the left hindlimb with one of two electrode placements.
889 Either with the anode placed under the tibial nerve and the cathode under the common peroneal nerve (CPN) to produce
890 Spillover (loaded) resistance exercise of the tibialis anterior or with both electrodes under the CPN to elicit concentric
891 (unloaded) resistance exercise or continuous low frequency stimulation to elicit endurance training).

892 Figure 2: An overview of the in-situ placement of the osmotic pump loaded with a pre-determined volume of tetrodotoxin
893 (TTX), placed in the scapula region with silicone tubing leading to the left hind-limb and the silicone cuff that encircled the
894 common peroneal nerve (CPN) to selectively block the ankle dorsiflexors, while maintaining normal plantarflexion.

895 Figure 3: Control tibialis anterior (TA) muscles. (A) Fiber type distribution, (B) Muscle fiber cross-sectional area, (C)
896 Myonuclei per fiber cross-section, (D) Myonuclear domain size. n = 32. (E) Total number of muscle fibers detected per mid-
897 belly transverse cross-section. n = 64. (F) Total number of muscle fibers detected between experimental condition groups
898 and their contralateral control limb. Note spread of control values in each group and small differences between left and
899 right limbs. *P ≤ 0.05. **P ≤ 0.01. ***P ≤ 0.001. ****P ≤ 0.0001. Mean ± Standard Deviation. (G) Example hematoxylin and
900 eosin staining of TA mid-belly cross-section following 14 days of TTX treatment for assessment of damage, degeneration,
901 and denervation. (H) Serial immunofluorescence section of G, depicting the deep oxidative portion toward the top right of
902 the transverse section (More green and red fibers). (Magenta = Dystrophin, Blue = Nuclei, Green = Type 1, Red = Type IIA,
903 Black Fibers = Type IIX/IIB). Scale bar = 2000μm. (I) Higher magnification of muscle fiber staining from deep oxidative
904 portion. Scale bar = 40μm.

905 Figure 4: changes in response to 7 days low frequency continuous stimulation: (A) Percentage change in muscle mass
906 between the left experimental tibialis anterior (TA) and right contralateral control TA, 7 days after sham surgery or after 7
907 days of continuous 24-hour low-frequency stimulation (CLFS). (B-D) Fiber CSA, myonuclei per fiber cross-section and
908 myonuclear domain size assessed across all muscle fibers, expressed as percentage change between left experimental TA
909 and right contralateral control TA for the same groups as in (A). (E-G) Fiber type proportions in control and after 7 days of
910 low frequency stimulation. (H-J) Fiber type-specific fiber CSA. (K-M) Fiber type specific myonuclei per fiber cross-section
911 measurements. (N-P) Fiber type specific myonuclear domain sizes. *P ≤ 0.05. **P ≤ 0.01. ***P ≤ 0.001. ****P ≤ 0.0001.
912 Mean ± Standard Deviation.

913 Figure 5: (A) Percentage change in muscle mass relative to body mass between the left experimental tibialis anterior (TA)
914 and right contralateral control TA, over a time course (2d, 10d, 20d, 30d) of Spillover(loaded) training or 30d of unloaded

915 resistance training. (B-D) Fiber CSA, myonuclei per fiber cross-section and myonuclear domain size assessed across all
916 muscle fibers, expressed as percentage change between left experimental TA and right contralateral control TA. (E-G) Fiber
917 type proportions in control, 30 days loaded resistance training and 30 days unloaded training. (H-J) Fiber type specific fiber
918 CSA. (K-M) Fiber type specific myonuclei per fiber cross-section measurements. (N-P) Fiber type-specific myonuclear
919 domain sizes. *P ≤ 0.05. **P ≤ 0.01. ***P ≤ 0.001. ****P ≤ 0.0001. Mean ± Standard Deviation.

920 Figure 6: (A) Percentage change in muscle mass between the left experimental tibialis anterior (TA) and right contralateral
921 control TA, over a time course (3d, 7d, 14d) of tetrodotoxin (TTX)-induced nerve silencing atrophy and subsequent
922 recovery through 7d habitual activity. (B-D) Fiber CSA, myonuclei per fiber cross-section and myonuclear domain size
923 assessed across all muscle fibers, expressed as percentage change between left experimental TA and right contralateral
924 control TA. (E-G) Fiber type proportions in control, following 14 days atrophy and following 14 days of atrophy with 7 days
925 of subsequent recovery. (H-J) Fiber type-specific fiber CSA. (K-M) Fiber type-specific myonuclei per fiber cross-section
926 measurements. (N-P) Fiber type-specific myonuclear domain sizes. *P ≤ 0.05. **P ≤ 0.01. ***P ≤ 0.001. ****P ≤ 0.0001.
927 Mean ± Standard Deviation.

928 Figure 7: (A-F) Correlations between percentage changes in muscle mass, muscle fiber CSA, myonuclei per fiber cross-
929 section and myonuclear domain size following a time course of loaded and unloaded resistance training. (G-L) Correlations
930 between percentage changes in muscle mass, muscle fiber CSA, myonuclei per fiber cross-section and myonuclear domain
931 size following a time course of TTX-induced atrophy. The subsequent 7-day recovery following 14 days of TTX induced
932 atrophy is expressed as the difference between the mean 14 days TTX value versus the individual 7-day recovery values.

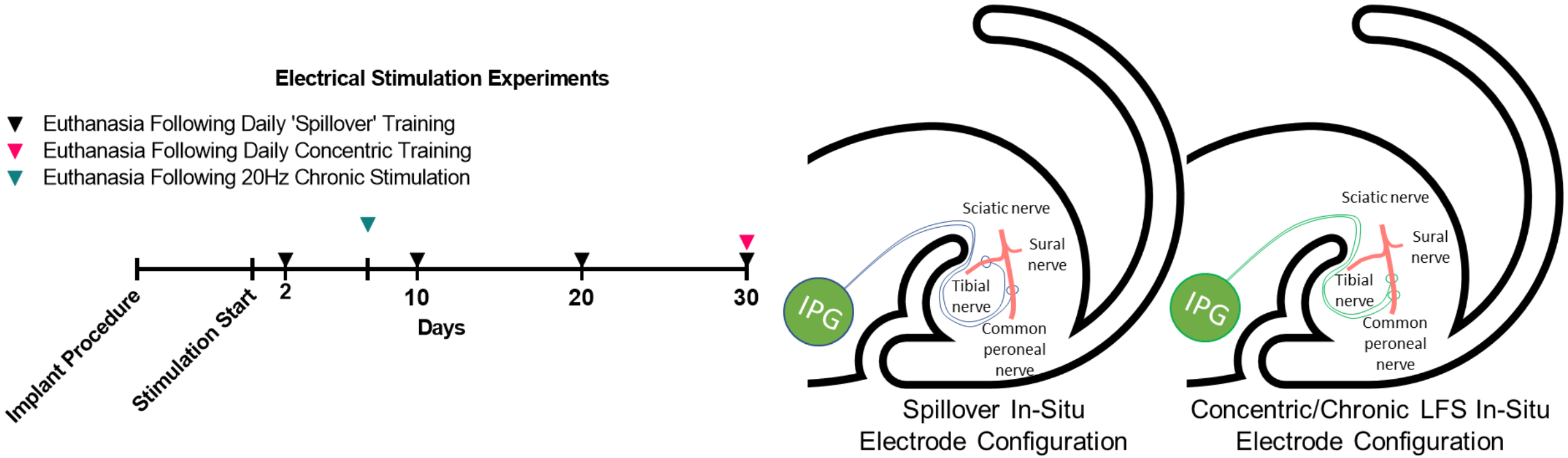

Nerve Silencing Experiments

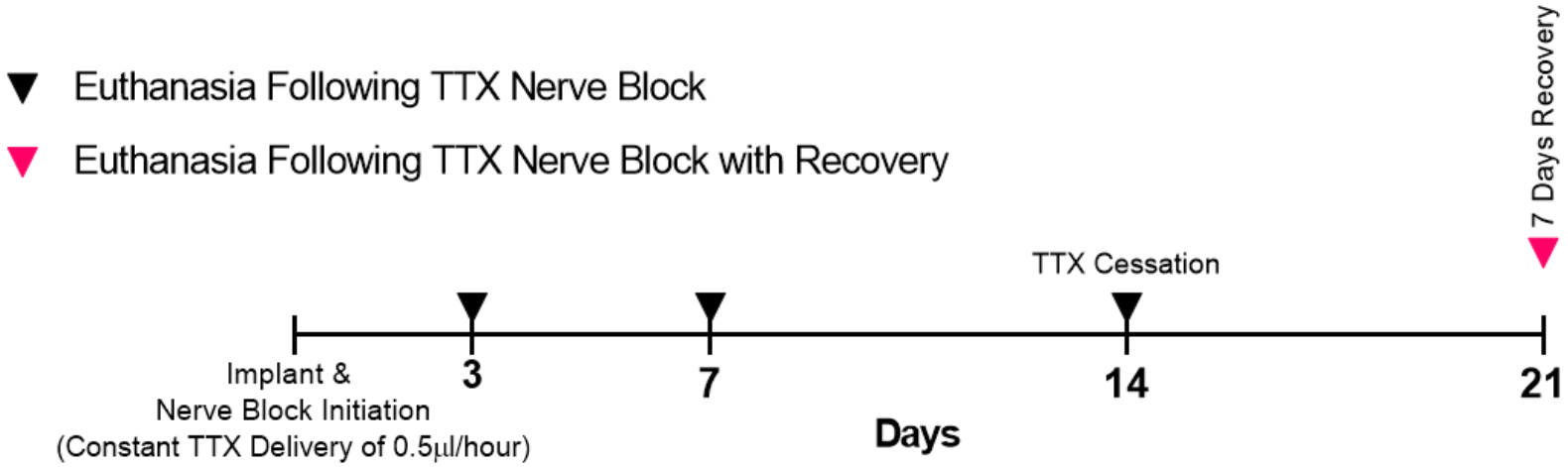

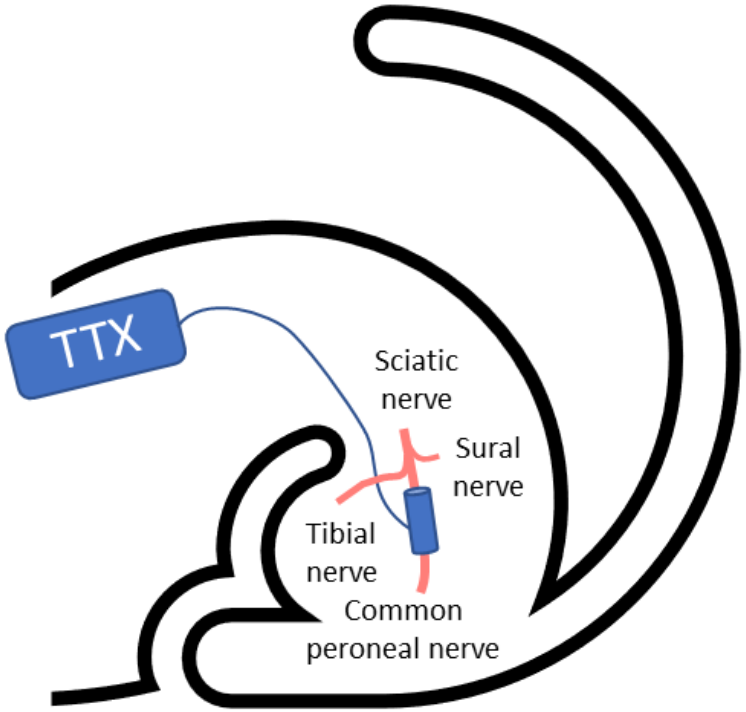

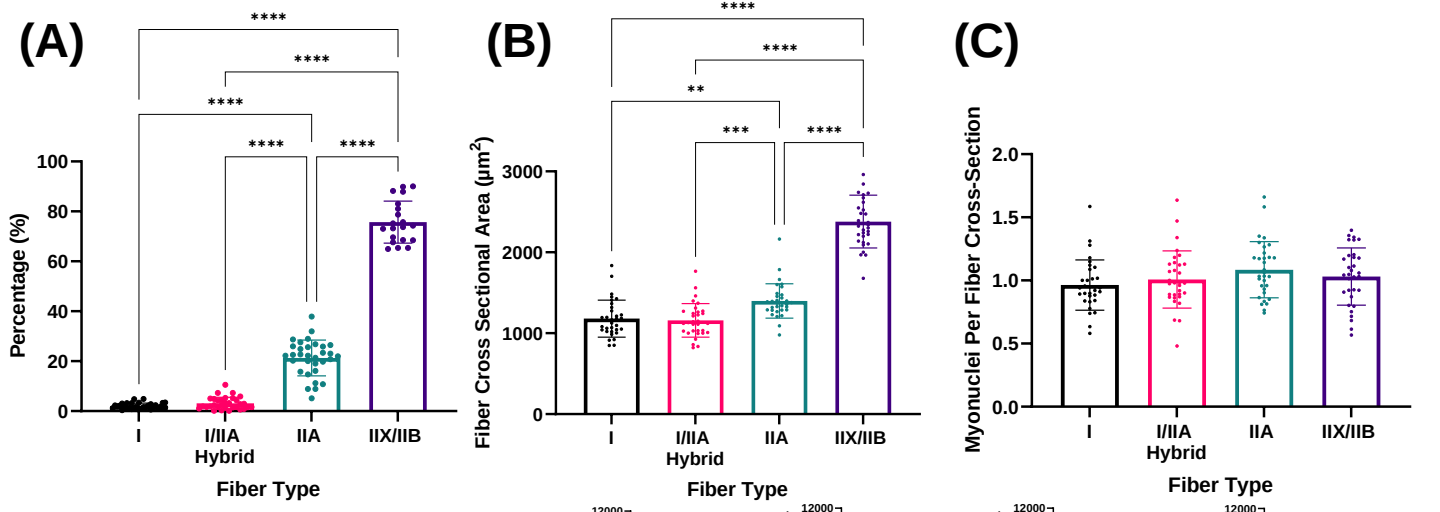

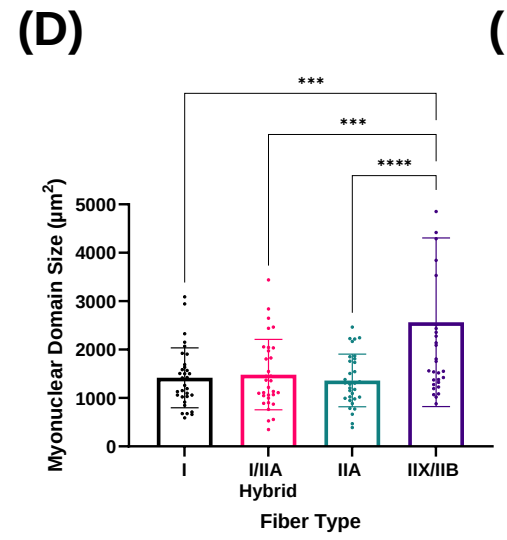

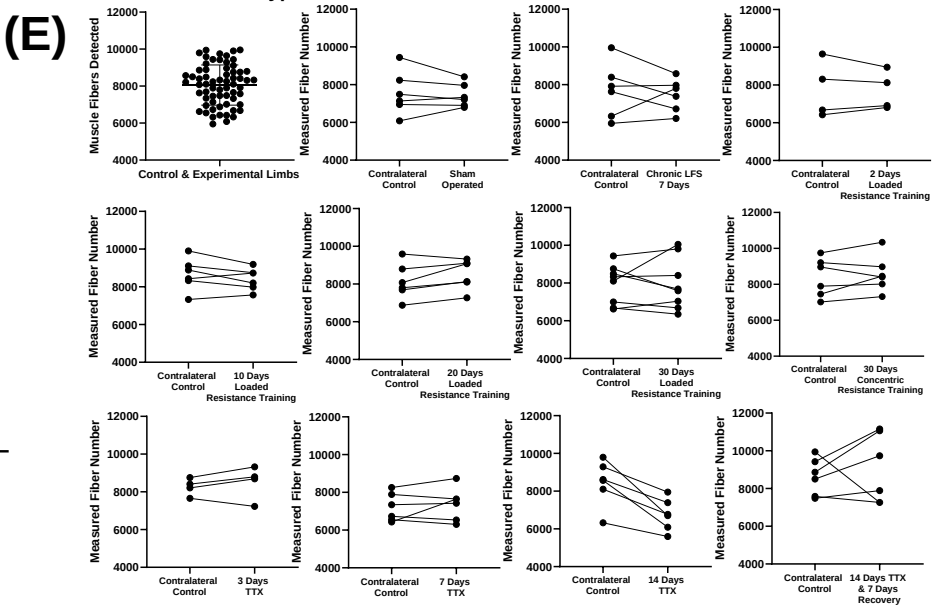

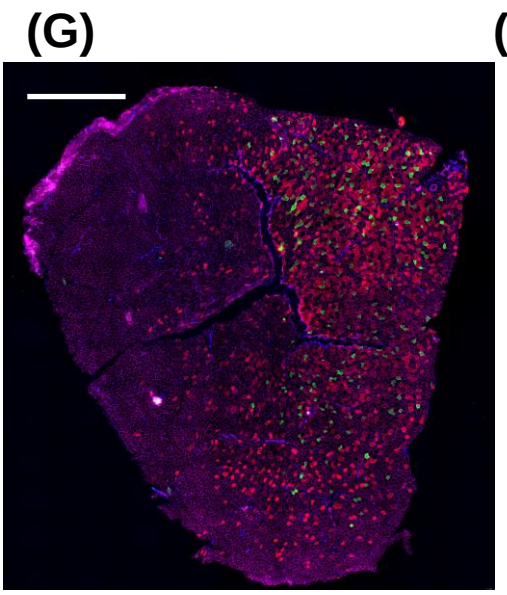

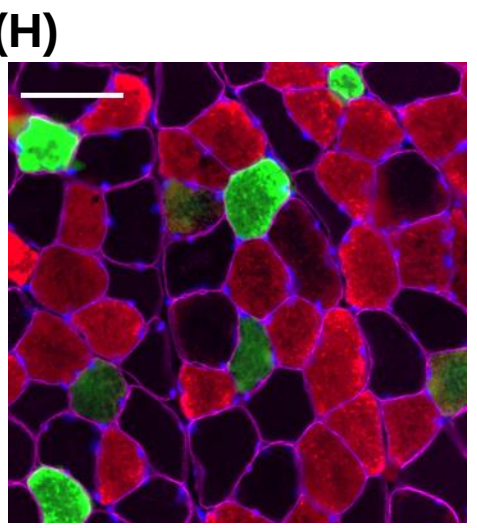

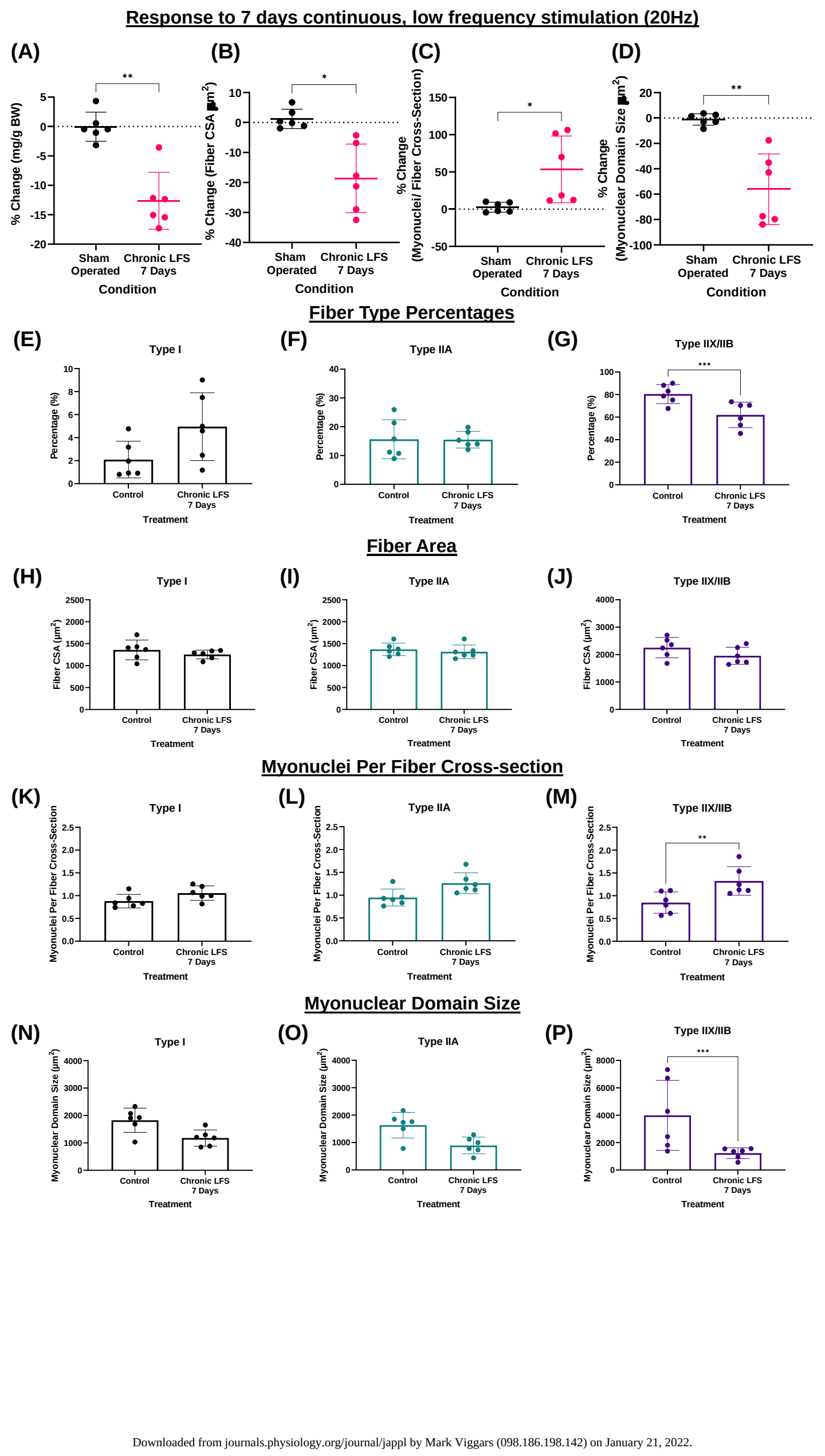

Time course response to loaded & unloaded resistance training

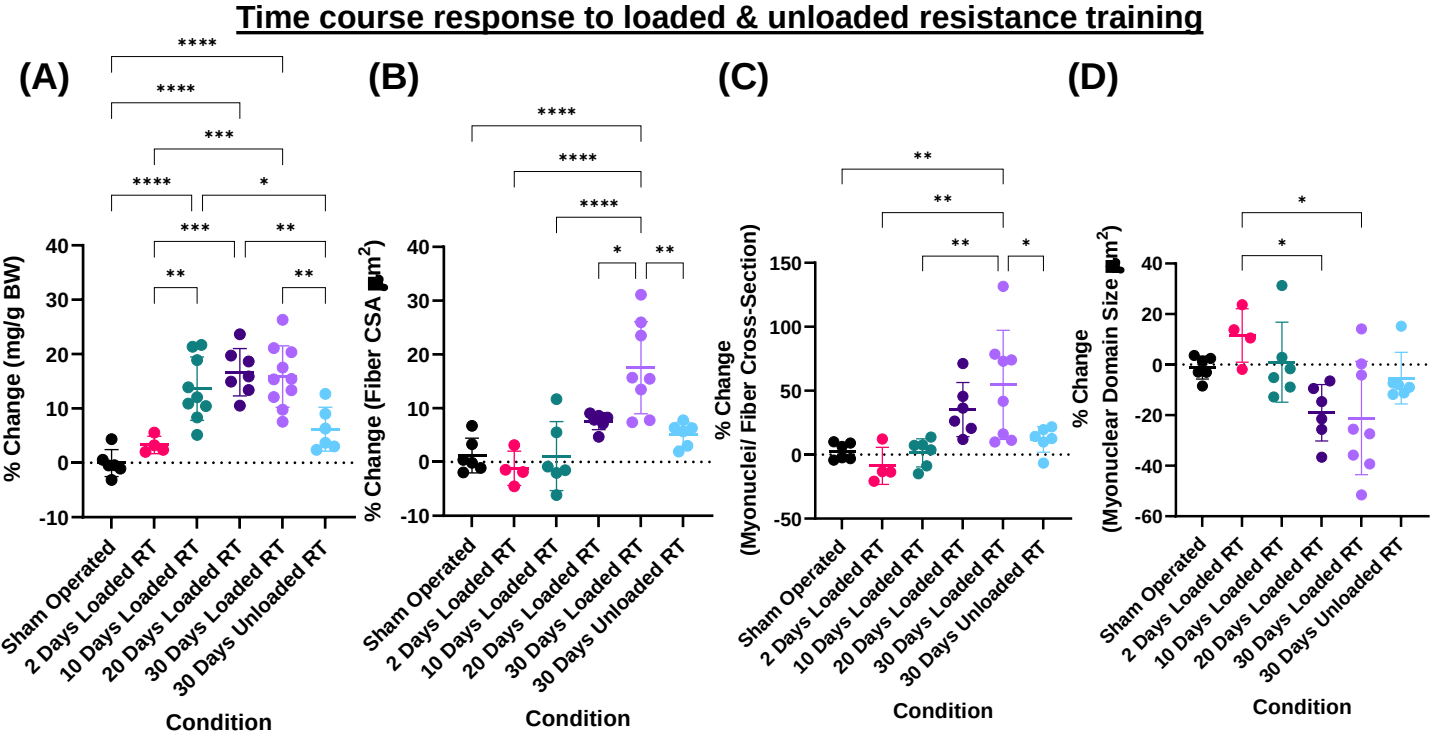

Fiber type percentages following 30 days of loaded and unloaded resistance training

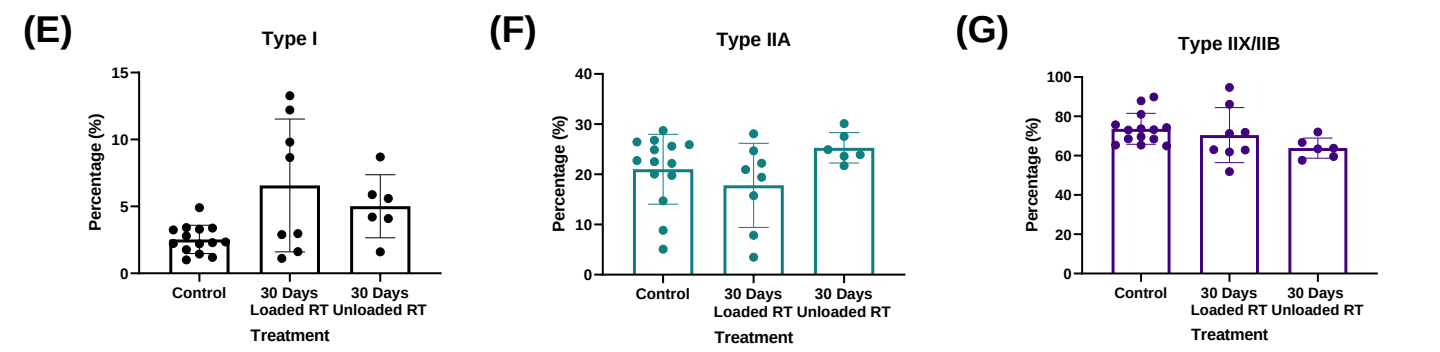

Fiber area following 30 days of loaded and unloaded resistance training

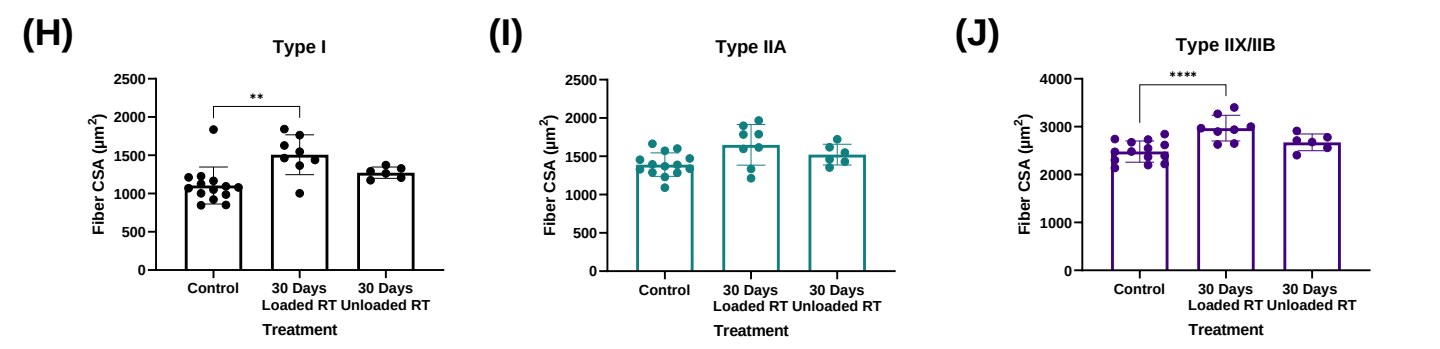

Myonuclei per fiber cross-section following 30 days of loaded and unloaded resistance training

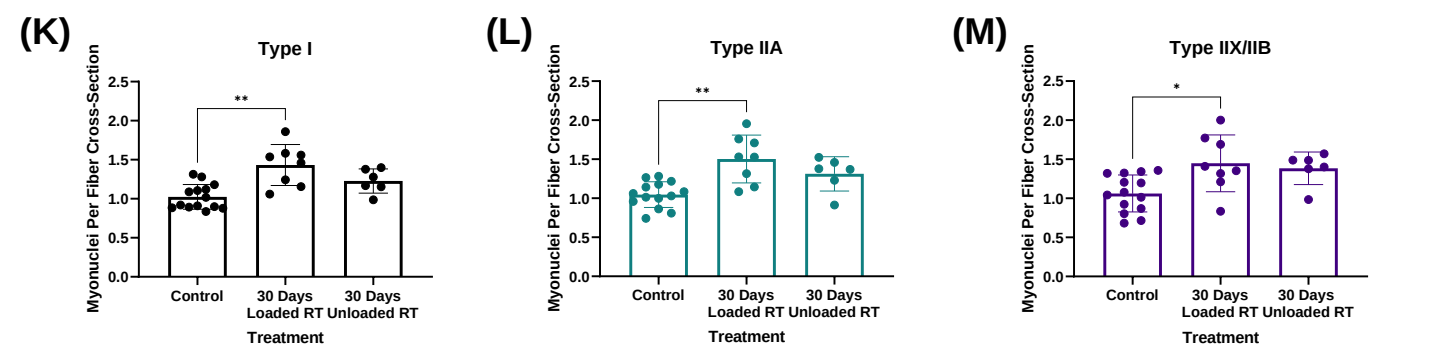

Myonuclear domain size following 30 days of loaded and unloaded resistance training

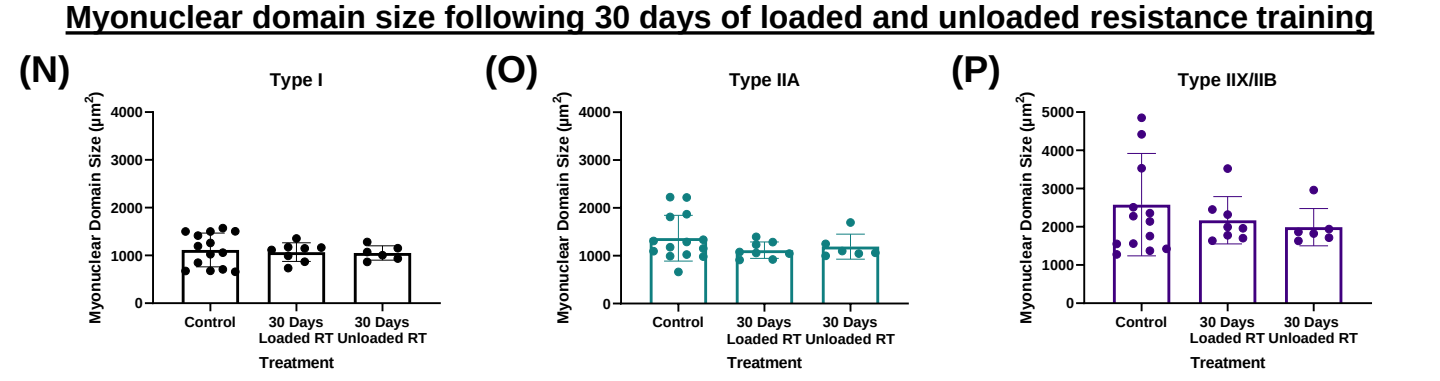

Time course response to TTX-induced atrophy and recovery

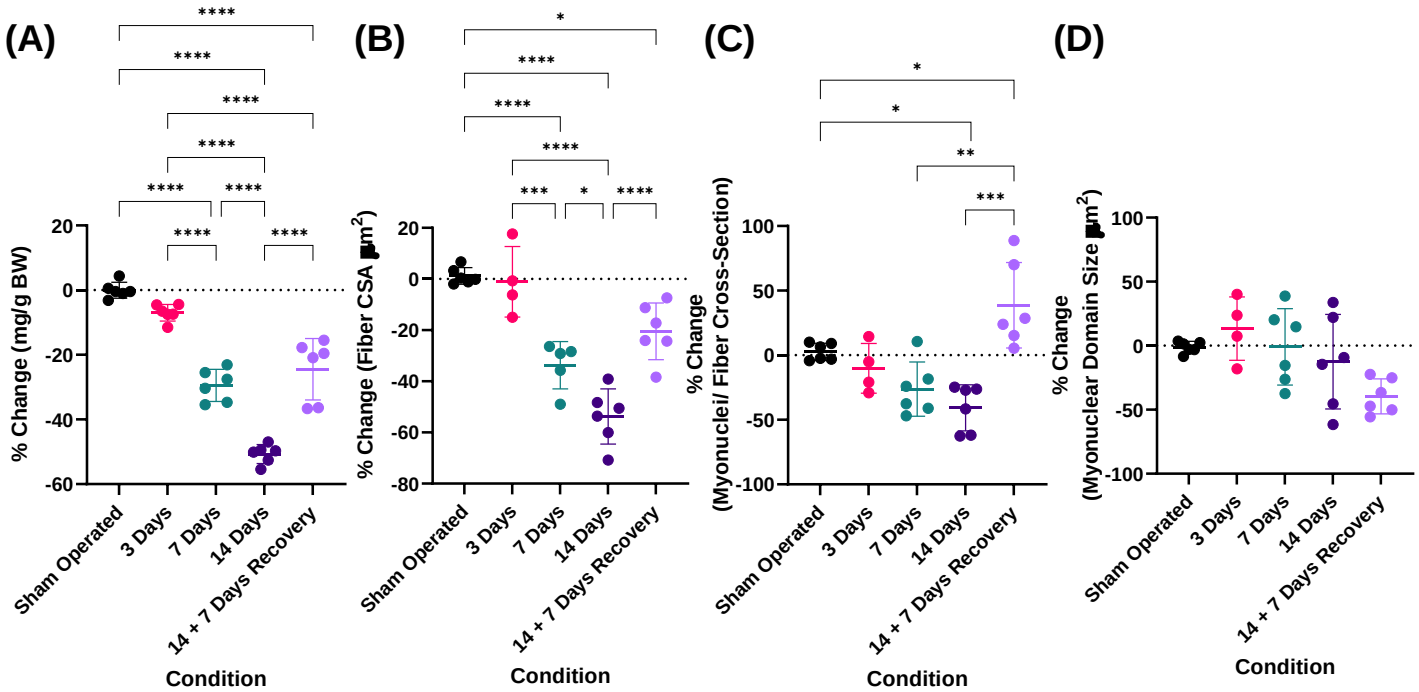

Fiber type percentages in disuse atrophy and recovery

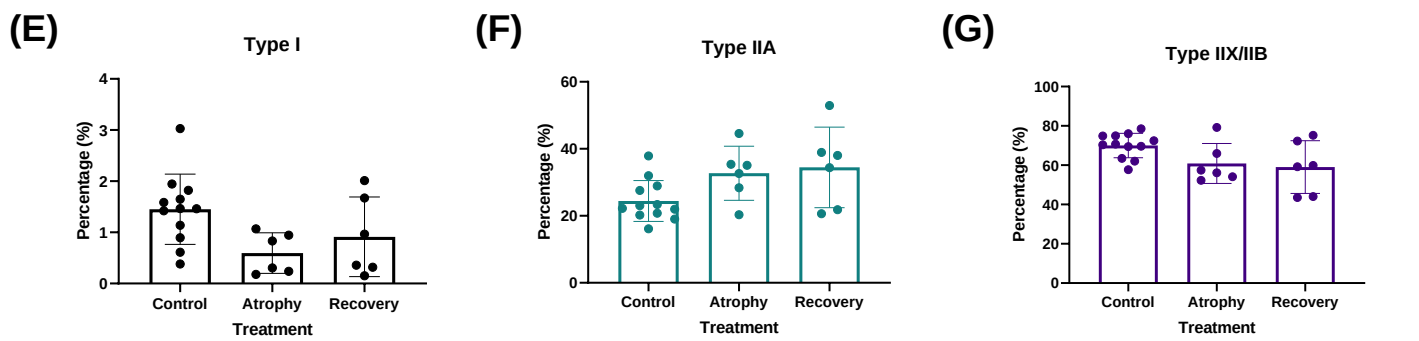

Fiber area in disuse atrophy and recovery

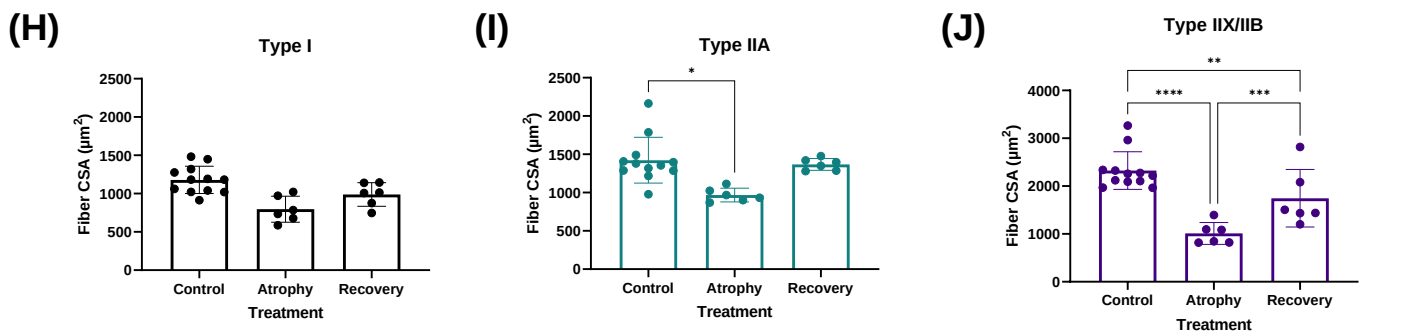

Myonuclei per fiber cross-section in disuse atrophy and recovery

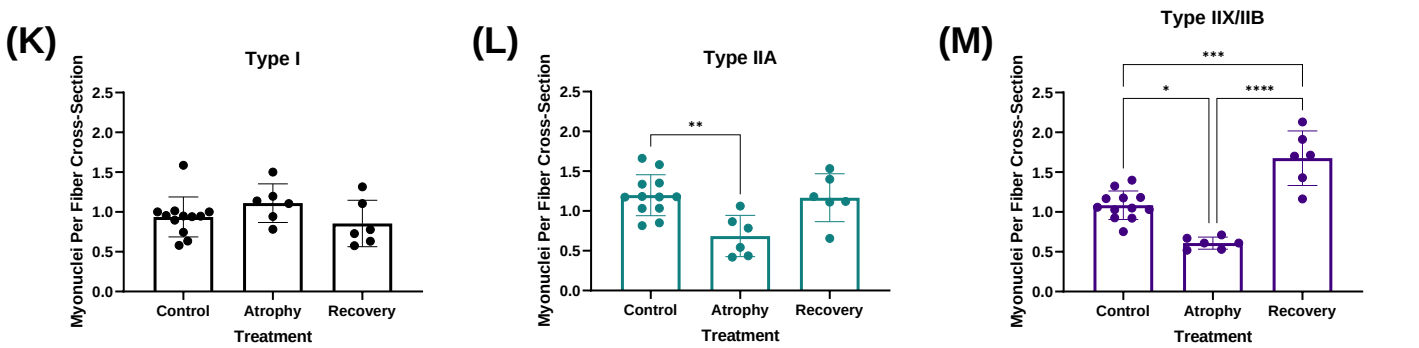

Myonuclear domain size in disuse atrophy and recovery

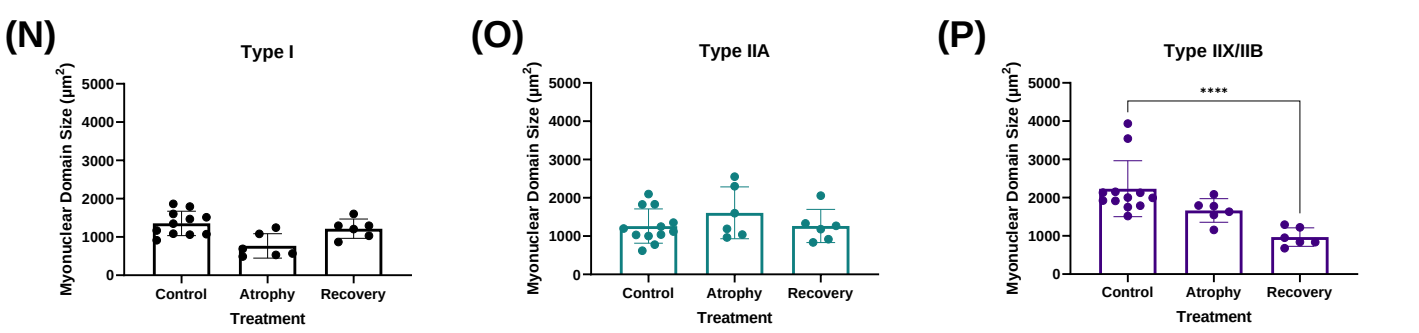

Correlations between adaptive responses to electrical stimulation-induced resistance training

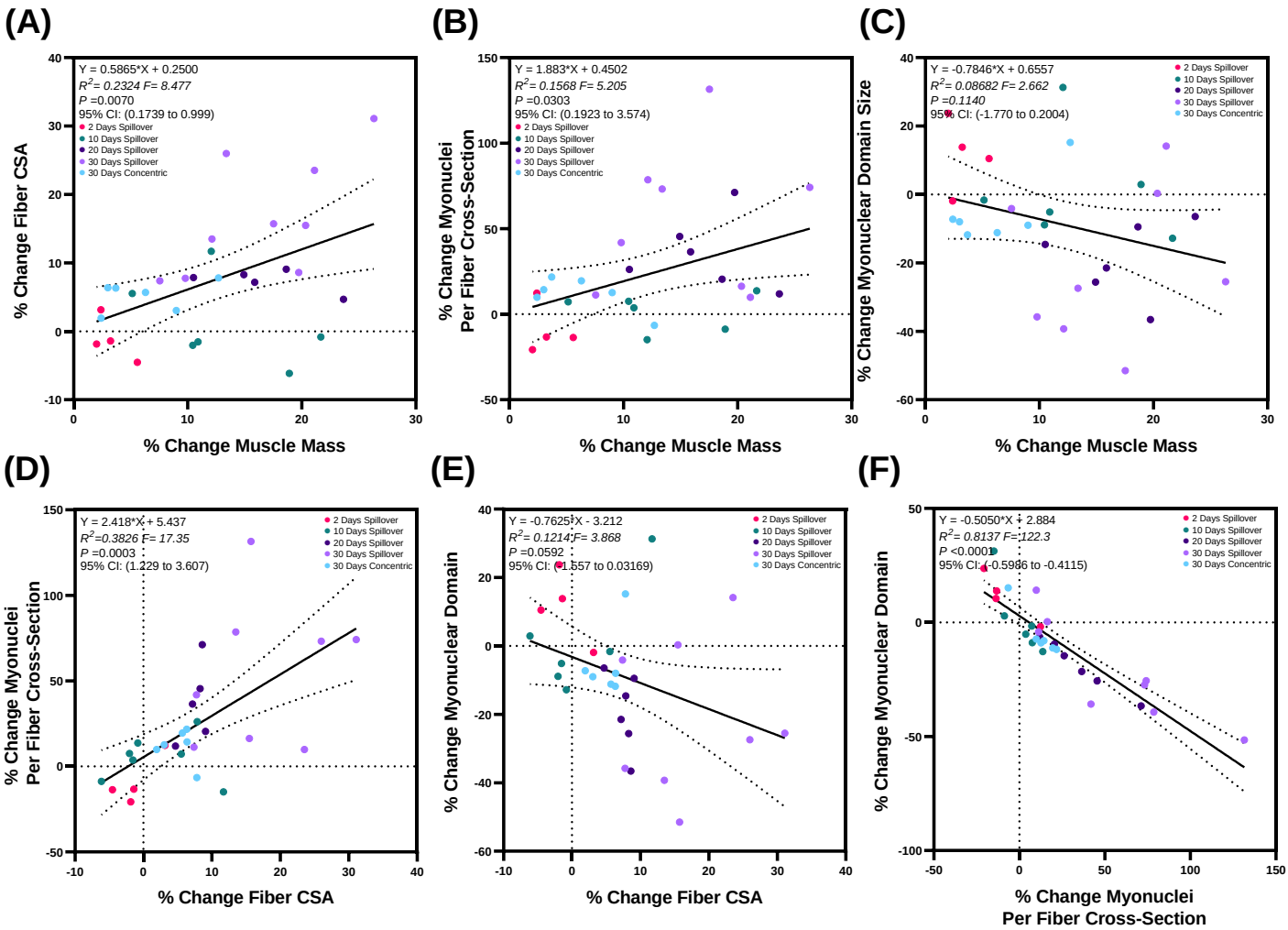

Correlations between adaptive responses to TTX induced atrophy and subsequent recovery

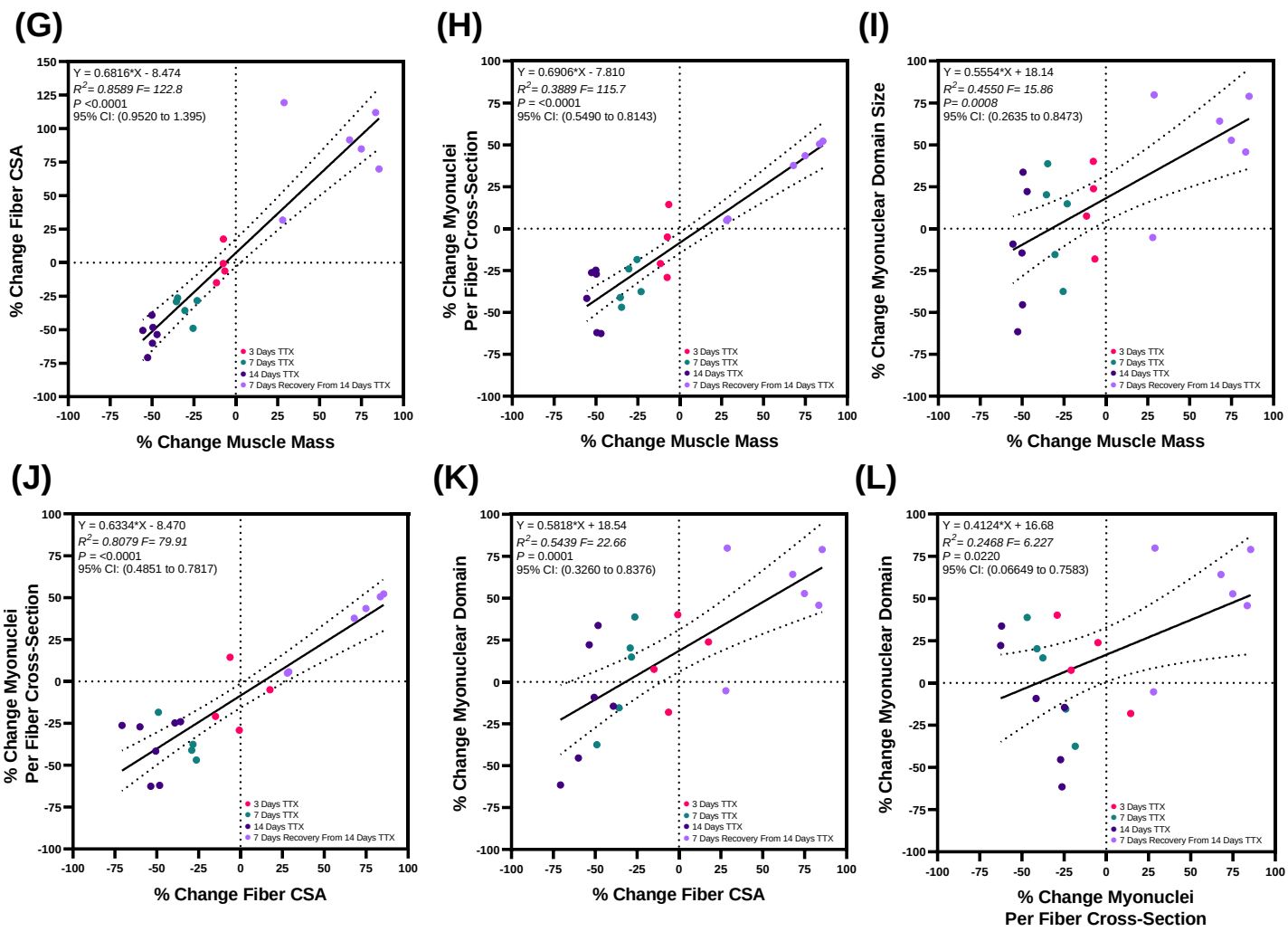

Primary Ab	Secondary Ab
MANDYS8(8H11) (Anti-dystrophin) DSHB Supernatant. Morris, G.E. (Developmental Studies Hybridoma Bank (DSHB) Hybridoma Product)	Goat anti-mouse IgG H&L (AlexaFluor® 594) preadsorbed Abcam (Cambridge, UK) (ab150120)
Dystrophin Polyclonal Antibody. Catalog #PA5-32388. (Thermofisher Scientific)	Goat anti-Rabbit IgG (H+L) Cross-Adsorbed Secondary Antibody, Alexa Fluor 633. A-21070 (Thermofisher Scientific)
BA-D5 (anti type I myosin) DSHB Supernatant. Schiaffino, S. (DSHB Hybridoma Product)	Goat anti-Mouse IgG2b Cross-Adsorbed Secondary Antibody, Alexa Fluor 488. A-21141 (Thermofisher Scientific)
SC-71 (anti type IIA myosin) DSHB Supernatant. Schiaffino, S. (DSHB Hybridoma Product)	Goat anti-Mouse IgG1 Cross-Adsorbed Secondary Antibody, Alexa Fluor 546. A-21123 (Thermofisher Scientific)

Table 1: Primary antibodies and appropriate corresponding secondary antibodies used.

Table 2: Body weight pre-surgery and post intervention for each experimental group.

Condition	Pre-Surgical Weight (M ± SD)	Post-Intervention Weight (M ± SD)
Sham Operated	443 ± 31	484 ± 78
CLFS 7 Days	397 ± 17	400 ± 20
2 Days Spillover	419 ± 58	411 ± 55
10 Days Spillover	382 ± 47	401 ± 52
20 Days Spillover	372 ± 34	416 ± 30
30 Days Spillover	413 ± 38	472 ± 52
30 Days Concentric	396 ± 33	415 ± 31
3 Days TTX	390 ± 12	416 ± 14
7 Days TTX	387 ± 22	420 ± 18
14 Days TTX	378 ± 11	417 ± 25
14 Days TTX + 7 Days Recovery	403 ± 35	452 ± 25
Mean	398	428
SD	20	27

Automated cross-sectional analysis of trained, severely atrophied and recovering rat skeletal muscles using MyoVision 2.0

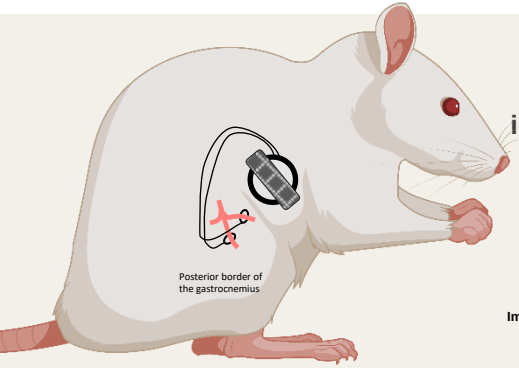

Free-living rats.
Daily resistance and continuous endurance training with implantable electrical stimulators.

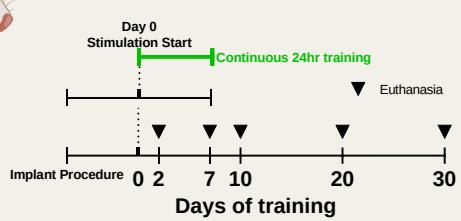

Free-living rats.
TTX-induced disuse atrophy and reversible nerve silencing with implantable osmotic pumps.

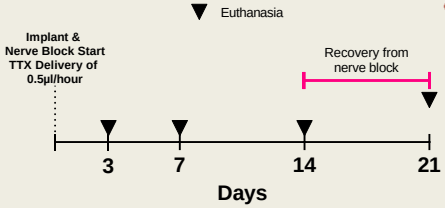

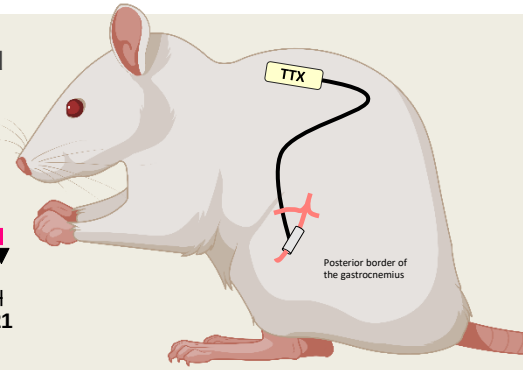

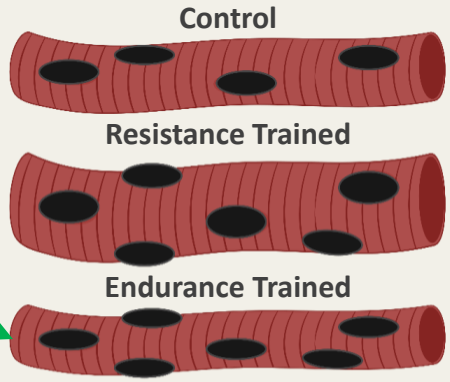

Fiber area hypertrophy (14%) with myonuclear addition (55%).

Fiber type shift & fiber area reduction (-18%) with myonuclear addition (53%).

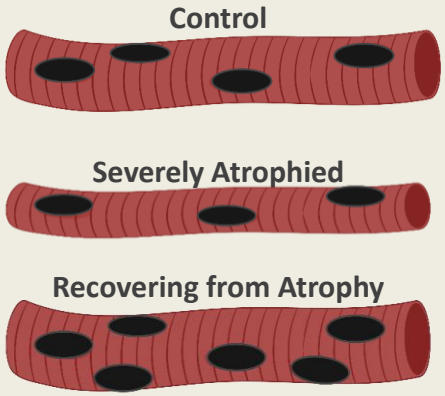

Reduction in fiber area (-54%) with a loss of myonuclei (-40%).

Substantial myonuclear addition (39%) observed with recovery of fiber area (73%) in type IIX/IIB fibers.

CONCLUSION: Myonuclei number per unit fiber length is not fixed and does not always correlate with fiber size. Myonuclear density appears to reflect the changes in activation and loading of the muscle fiber. Type IIX/IIB fibers show greater plasticity than slower types.